Supplementary material for LHCb-PAPER-2016-030

This appendix contains supplementary material that will be posted on the public CDS record but will not appear in the paper.

The asymmetry measurements, $a_P^{\widehat{T}\text{-odd}}$ and $a_{CP}^{\widehat{T}\text{-odd}}$, are shown in Fig. 5 in bins of $|\Phi|$ of the control sample $\Lambda_b^0 \to \Lambda_c^+\pi^-$. At the bottom of each plot, the numerical result of a χ^2 test calculated with respect to the null hypothesis is shown. The large χ^2/ndf value for the $a_P^{\widehat{T}\text{-odd}}$ measurements, corresponding to a p-value of 1.4×10^{-18}, indicates significant PV in the control channel. The p-value for CP symmetry is 0.14. The uncertainties are statistical only.

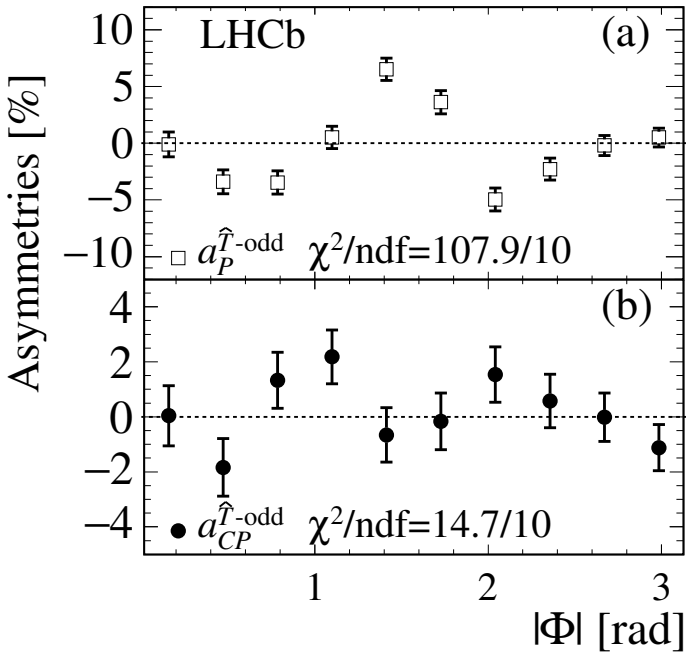

Figure 5: The distribution of the triple-product asymmetries (a) $a_P^{\widehat{T}\text{-odd}}$ and (b) $a_{CP}^{\widehat{T}\text{-odd}}$ with respect to the angle Φ defined by the decay plane of the pK^- and $\pi^+\pi^-$ pairs of the $\Lambda_b^0 \to \Lambda_c^+\pi^-$ control sample.

The distributions for some relevant mass and $|\Phi|$ projections of $\Lambda_b^0 \to p\pi^-\pi^+\pi^-$ and $\Lambda_b^0 \to p\pi^-K^+K^-$ are shown in Figs. 6, 7 and 8, respectively. These plots are background-subtracted using the *sPlot* method and are not corrected for efficiency. Therefore they should be used for illustrative purposes only.

The results of the simultaneous fit of the integrated distributions of $\Lambda_b^0 \to p\pi^-\pi^+\pi^-$ and $\Lambda_b^0 \to p\pi^-K^+K^-$ in the subsamples defined by Λ_b^0 flavour and $C_{\widehat{T}}$ ($\overline{C}_{\widehat{T}}$) sign are shown in Fig. 9 and Fig. 10, respectively.

The results of the simultaneous fit of the events in each bin of scheme A are shown in Figs. 11-22.

The results of the simultaneous fit of the events in each bin of scheme B, in the regions $(i-1)\pi/10 < |\Phi| < (i)\pi/10$, with $i = 1, 2, ..., 10$, are shown in Figs. 23-32.

The results of the simultaneous fit to the $\Lambda_b^0 \to p\pi^-K^+K^-$ events in bin 1 are shown in Fig. 33, while those from bin 2 are in Fig. 34.

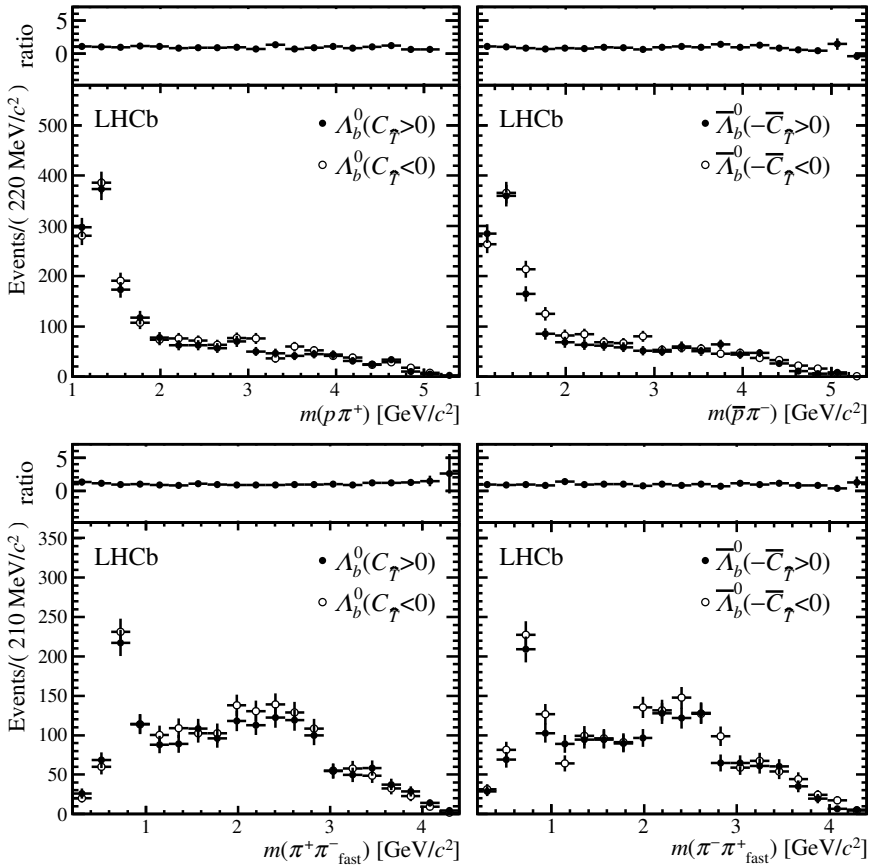

Figure 6: The projections of the signal events in the invariant mass of various combinations of particles in the final state for $\Lambda_b^0 \to p\pi^-\pi^+\pi^-$ decays. For each plot, the ratio of events with positive to negative $C_{\widehat{T}}$ (or $-\overline{C}_{\widehat{T}}$ for $\overline{\Lambda}_b^0$) is shown.

The fit to the invariant mass distribution of the $\Lambda_b^0 \to \Lambda_c^+(\to pK^-\pi^+)\pi^-$ control sample is shown in Fig. 35.

The χ^2 distribution of pseudoexperiments with *CP* symmetry in schemes A and B for $\Lambda_b^0 \to p\pi^-\pi^+\pi^-$ and the distribution of the $\log_{10}$ of the product of the p-values of schemes A and B are shown in Figure 36.

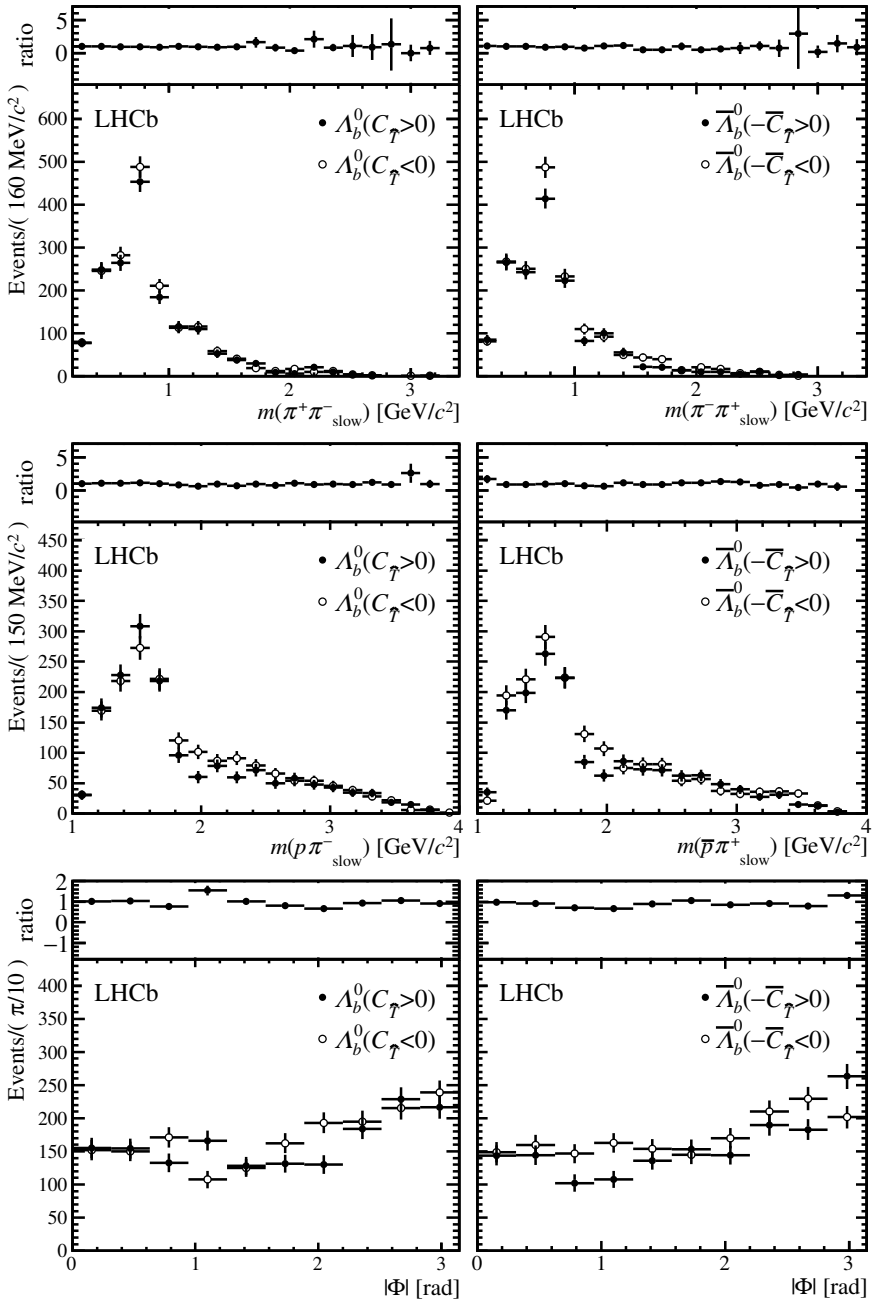

Figure 7: The projections of the signal events in the invariant mass of various combinations of particles in the final state and in $|\Phi|$ for $\Lambda_b^0 \to p\pi^-\pi^+\pi^-$ decays. For each plot, the ratio of events with positive to negative $C_{\widehat{T}}$ (or $-\overline{C}_{\widehat{T}}$ for $\overline{\Lambda}_b^0$) is shown.

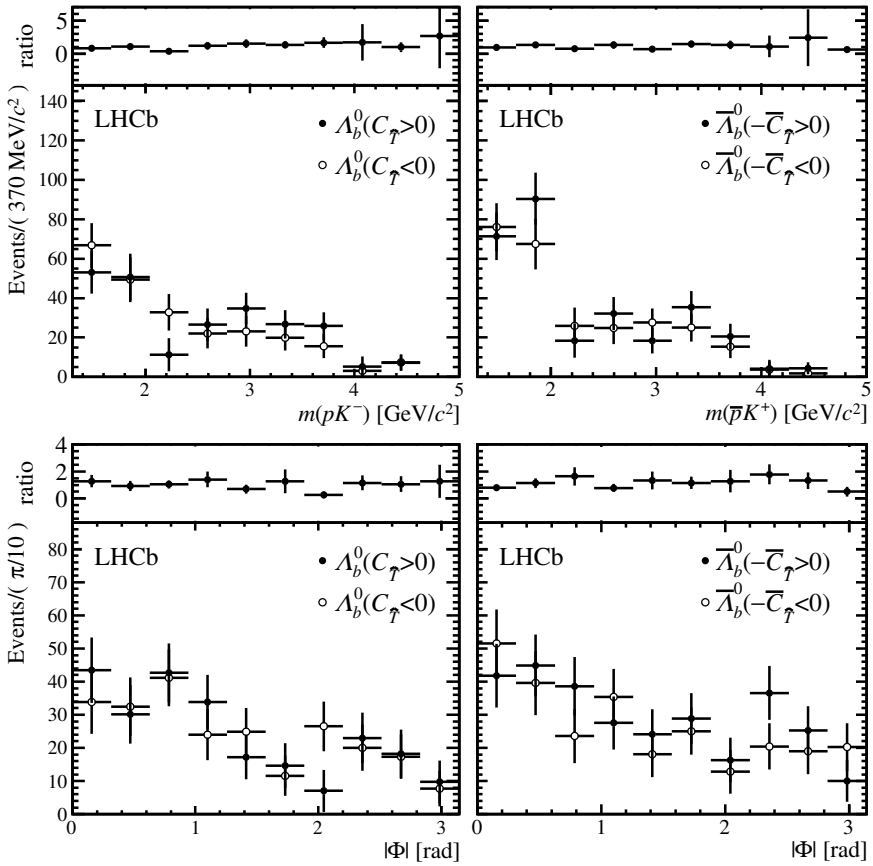

Figure 8: The projections of the signal events in the invariant mass of various combinations of particles in the final state and in $|\Phi|$ for $\Lambda_b^0 \to p\pi^- K^+ K^-$ decays. For each plot, the ratio of events with positive to negative $C_{\widehat{T}}$ (or $-\overline{C}_{\widehat{T}}$ for $\overline{\Lambda}_b^0$) is shown.

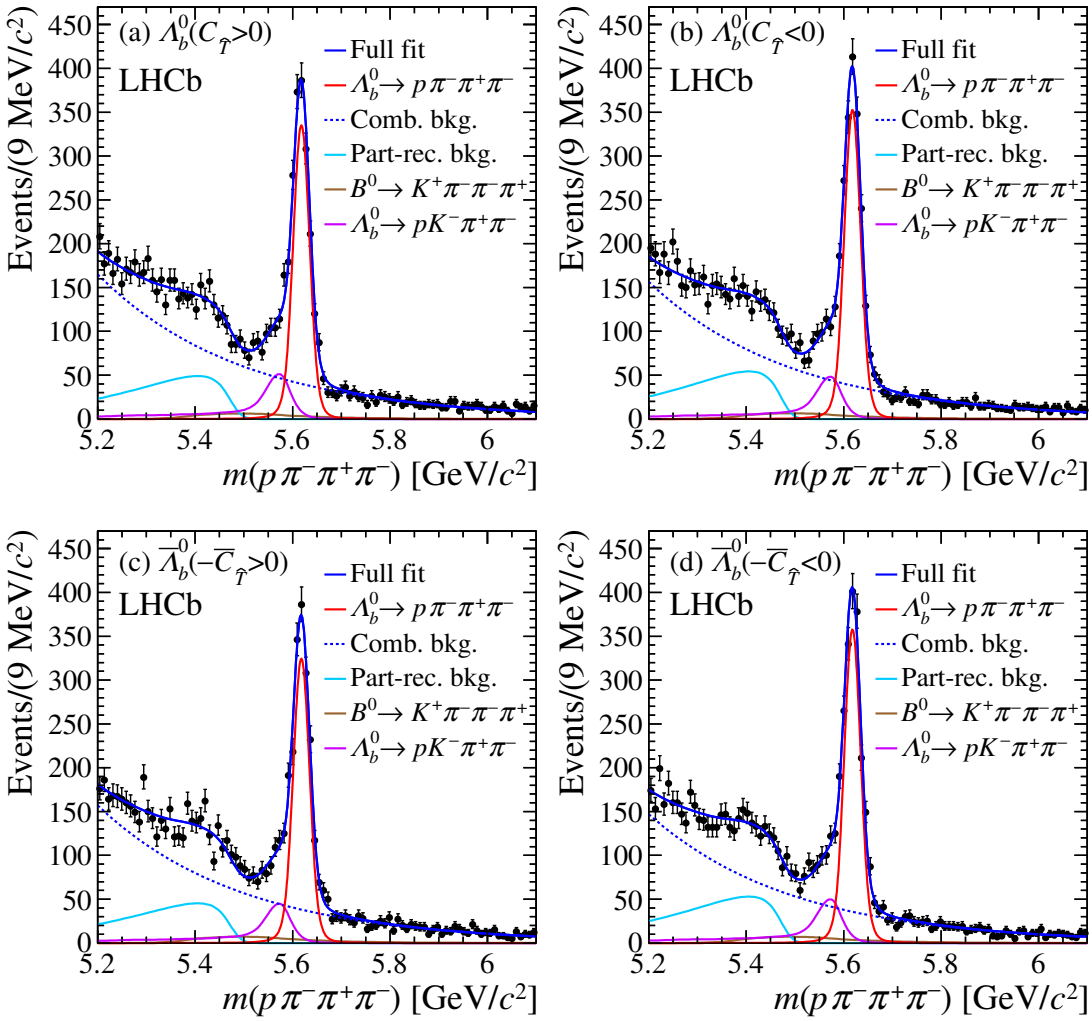

Figure 9: Projections of the unbinned maximum likelihood fit to the $\Lambda_b^0 \to p\pi^-\pi^+\pi^-$ decays in the four subsamples defined by Λ_b^0 flavour and $C_{\hat{T}}$ ($\overline{C}_{\hat{T}}$) sign. The data correspond to the entire phase space.

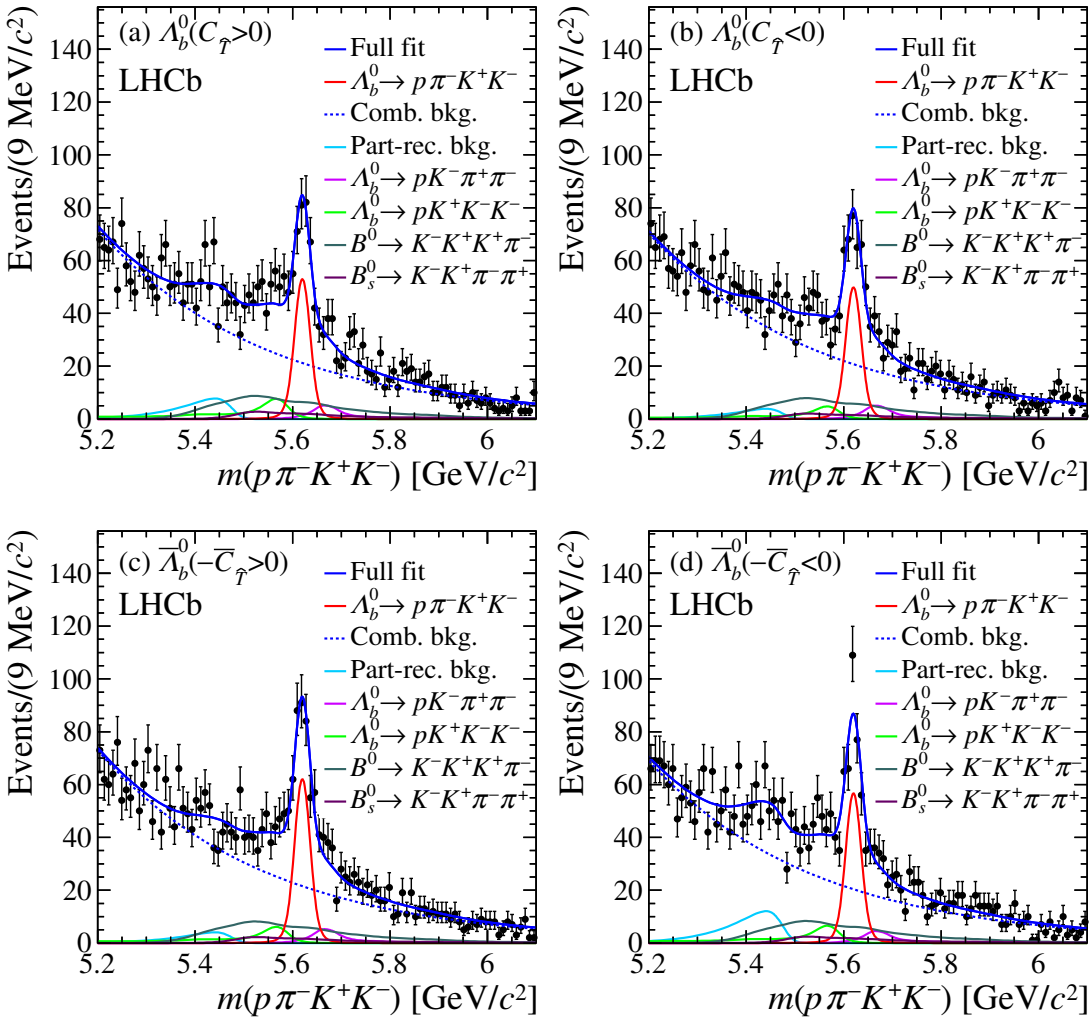

Figure 10: Projections of the unbinned maximum likelihood fit to the $\Lambda_b^0 \to p\pi^- K^+ K^-$ decays in the four subsamples defined by Λ_b^0 flavour and $C_{\widehat{T}}$ ($\overline{C}_{\widehat{T}}$) sign. The data correspond to the entire phase space.

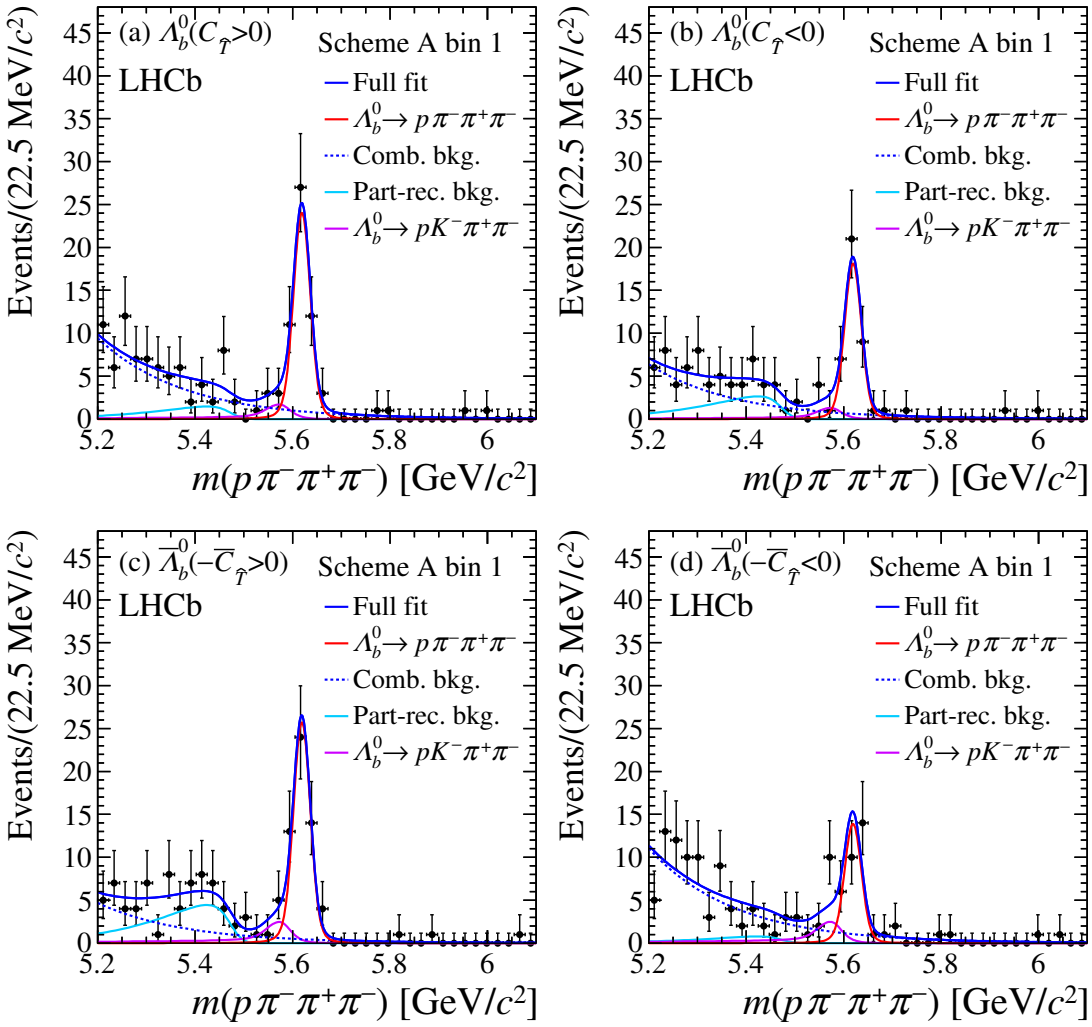

Figure 11: Projections of the unbinned maximum likelihood fit to the $\Lambda_b^0 \to p\pi^-\pi^+\pi^-$ decays in bin 1 in scheme A.

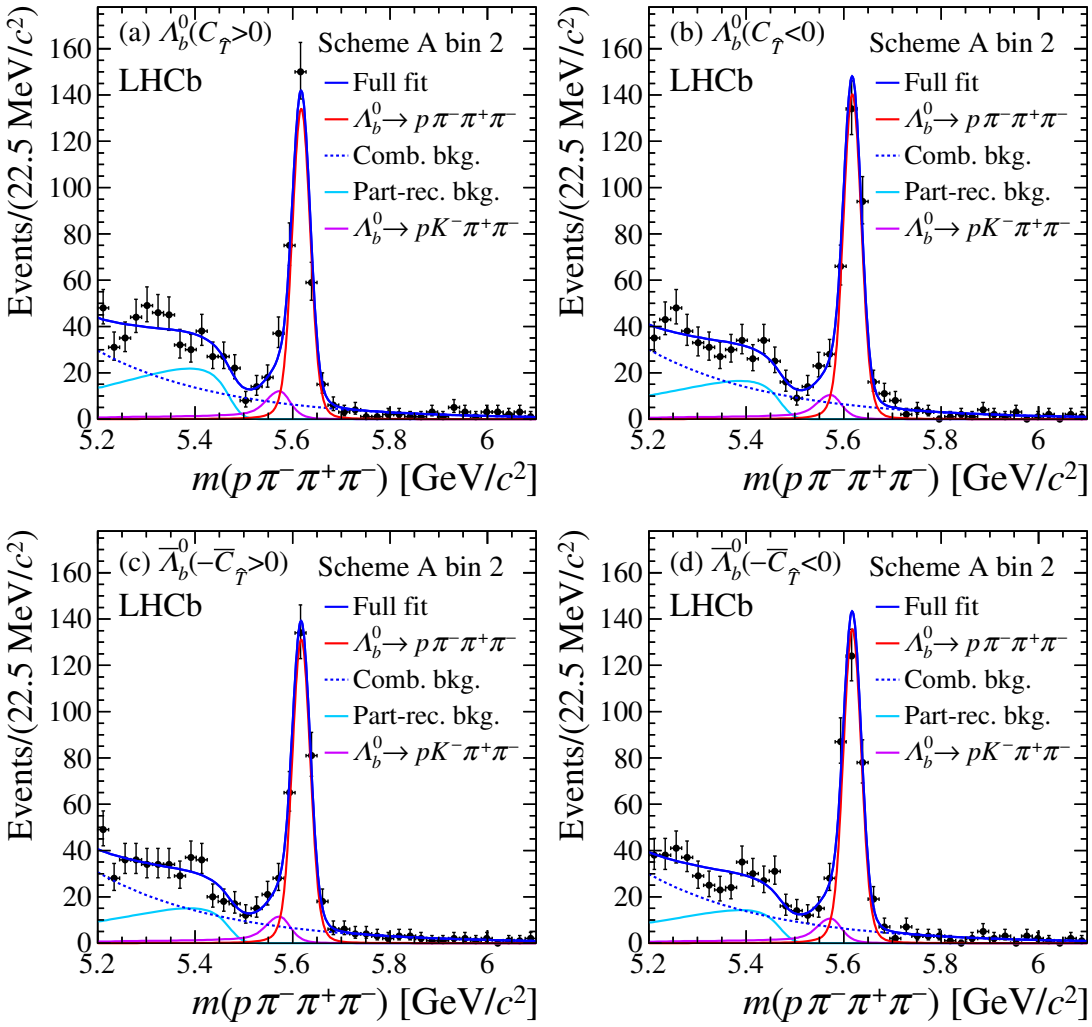

Figure 12: Projections of the unbinned maximum likelihood fit to the $\Lambda_b^0 \to p\pi^-\pi^+\pi^-$ decays in bin 2 in scheme A.

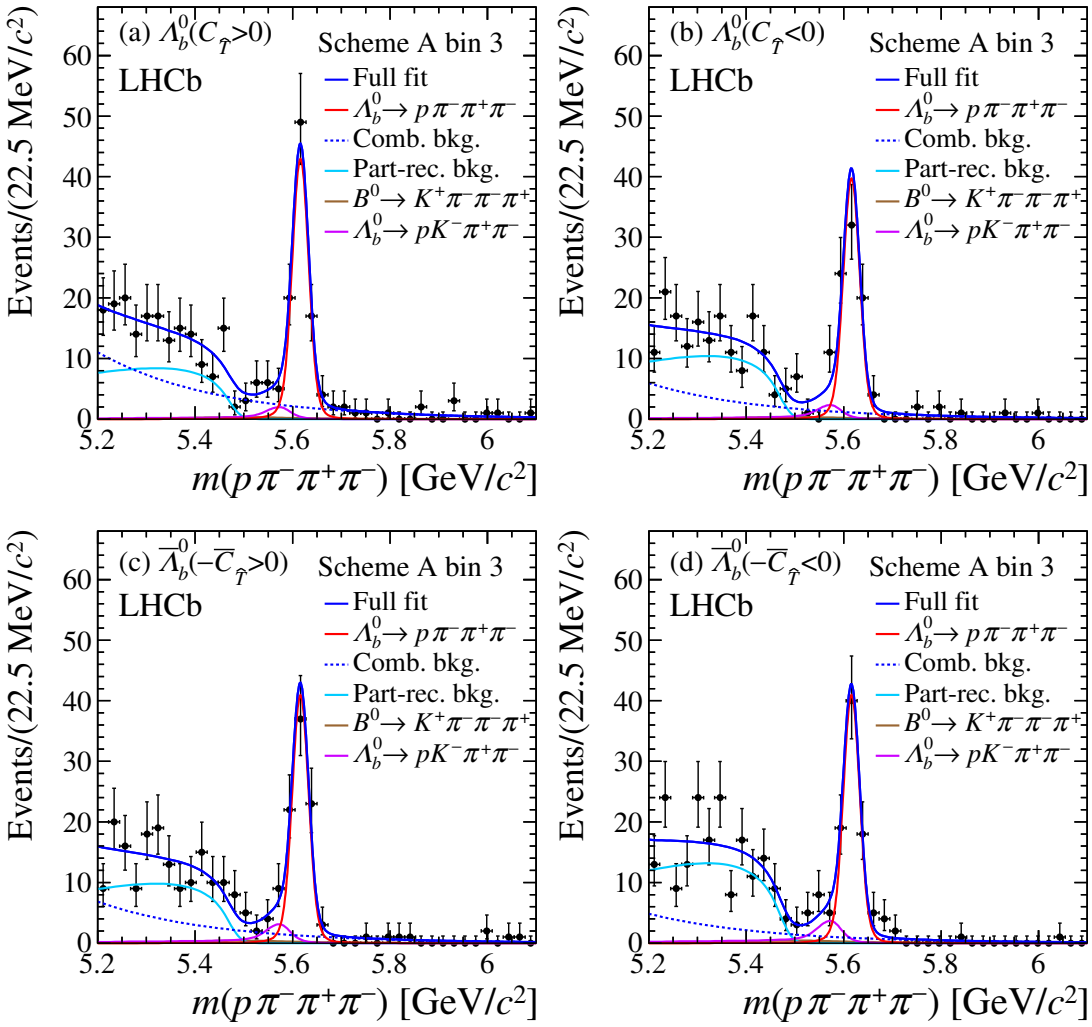

Figure 13: Projections of the unbinned maximum likelihood fit to the $\Lambda_b^0 \to p\pi^-\pi^+\pi^-$ decays in bin 3 in scheme A.

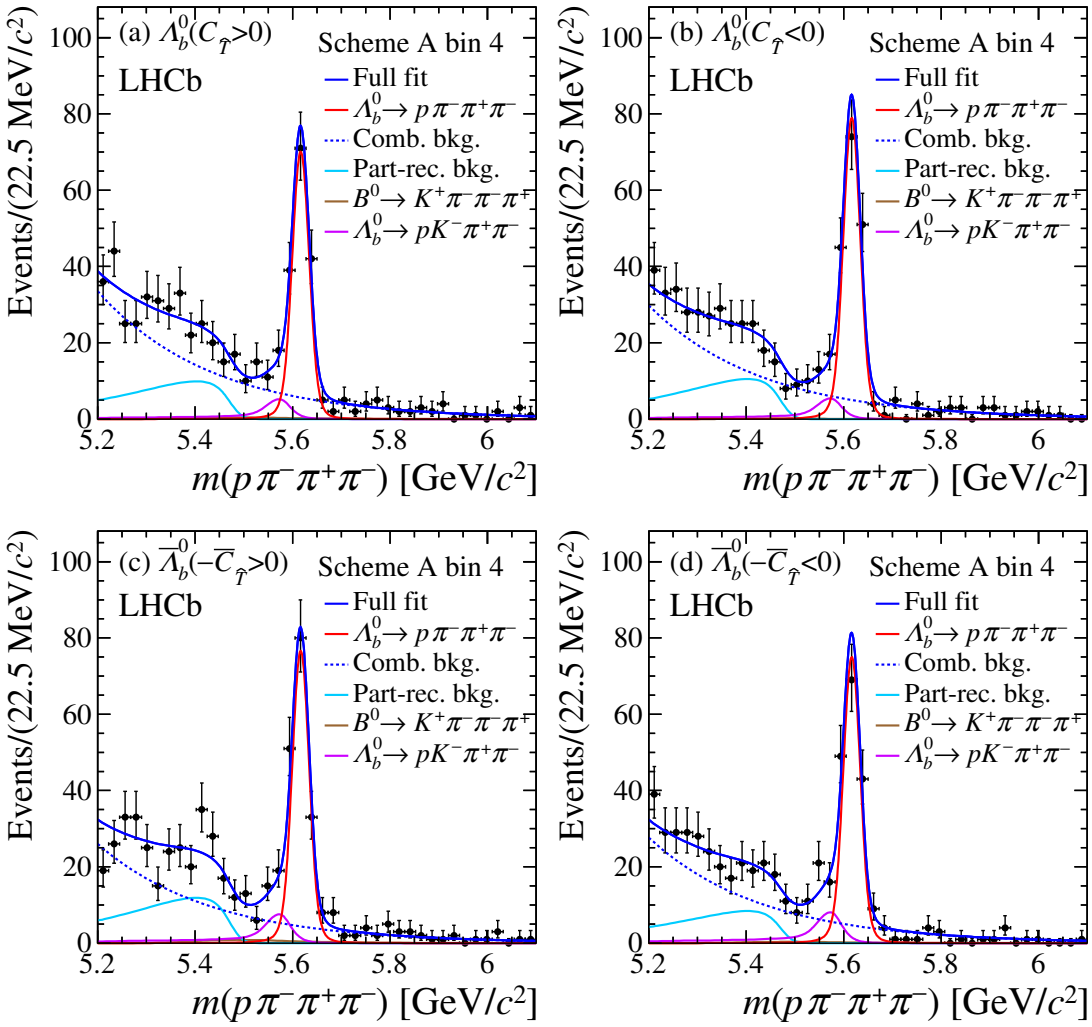

Figure 14: Projections of the unbinned maximum likelihood fit of the $\Lambda_b^0 \to p\pi^-\pi^+\pi^-$ decays in bin 4 in scheme A.

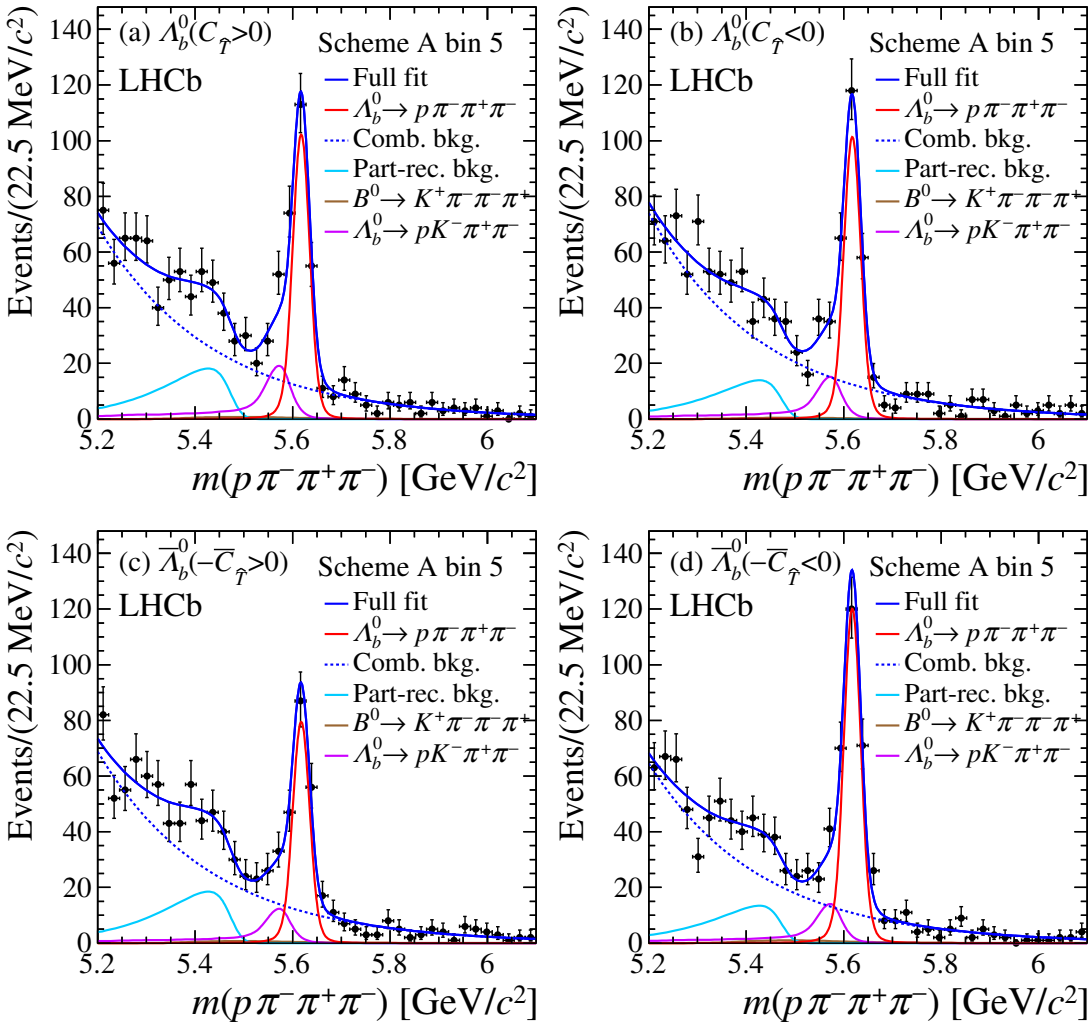

Figure 15: Projections of the unbinned maximum likelihood fit to the $\Lambda_b^0 \to p\pi^-\pi^+\pi^-$ decays in bin 5 in scheme A.

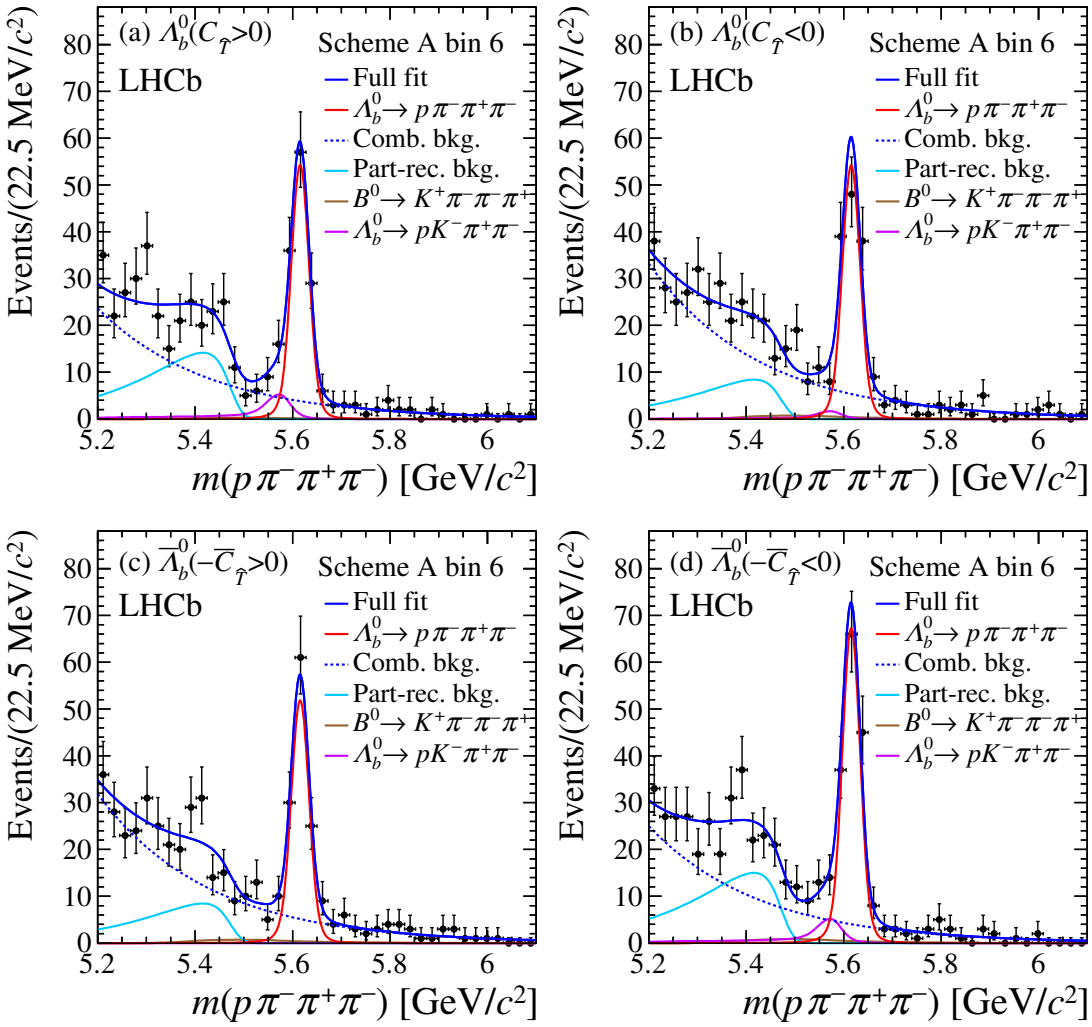

Figure 16: Projections the unbinned maximum likelihood fit to the $\Lambda_b^0 \to p\pi^-\pi^+\pi^-$ decays in bin 6 in scheme A.

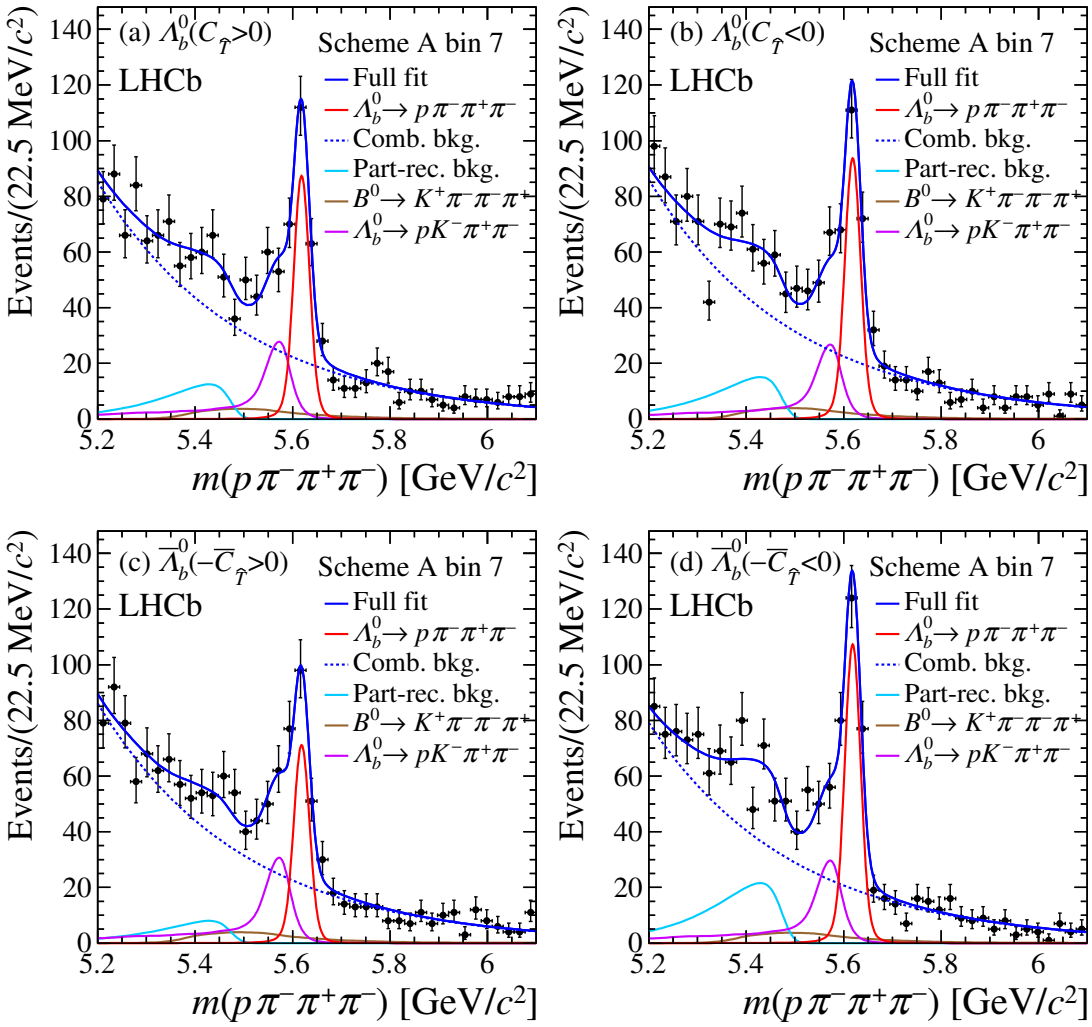

Figure 17: Projections of the unbinned maximum likelihood fit to the $\Lambda_b^0\to p\pi^-\pi^+\pi^-$ decays in bin 7 in scheme A.

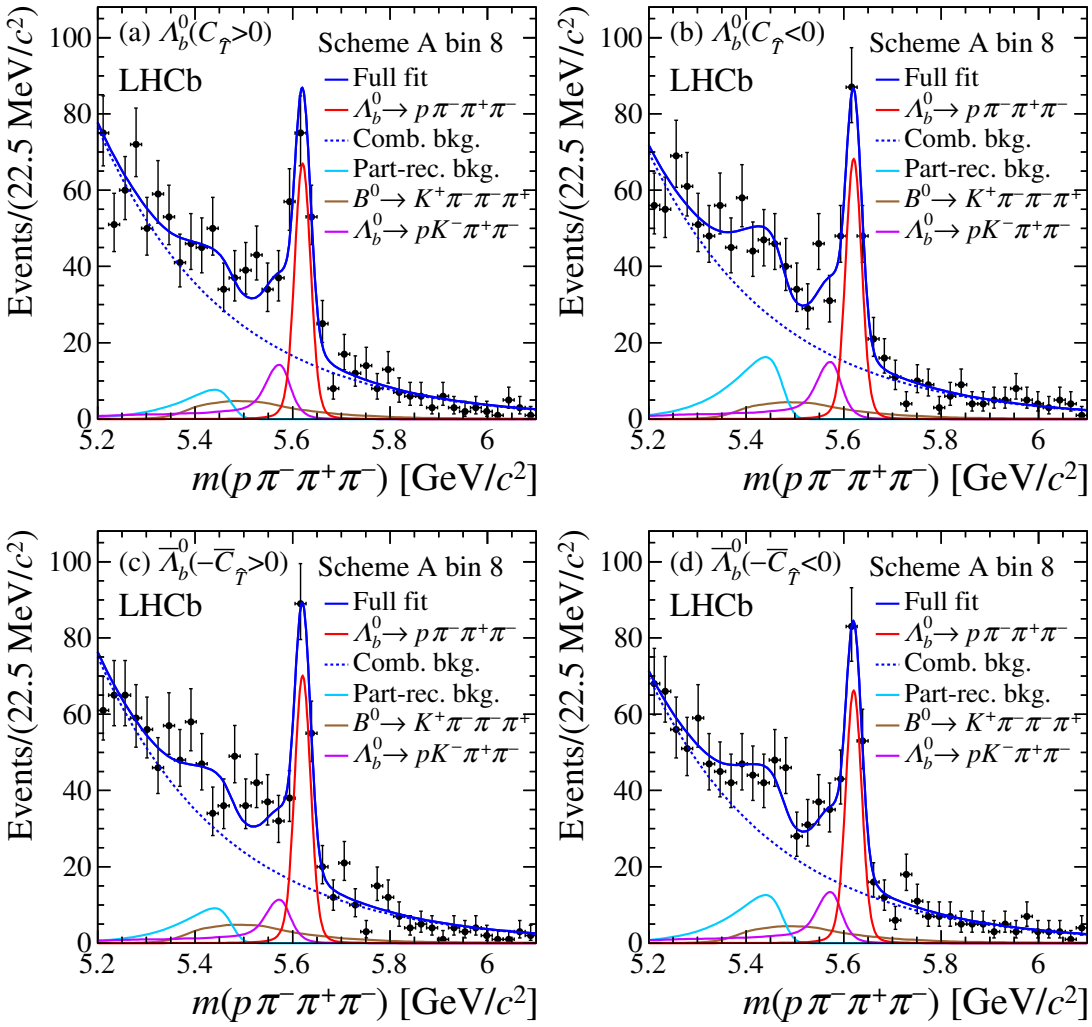

Figure 18: Projections of the unbinned maximum likelihood fit to the $\Lambda_b^0 \to p\pi^-\pi^+\pi^-$ decays in bin 8 in scheme A.

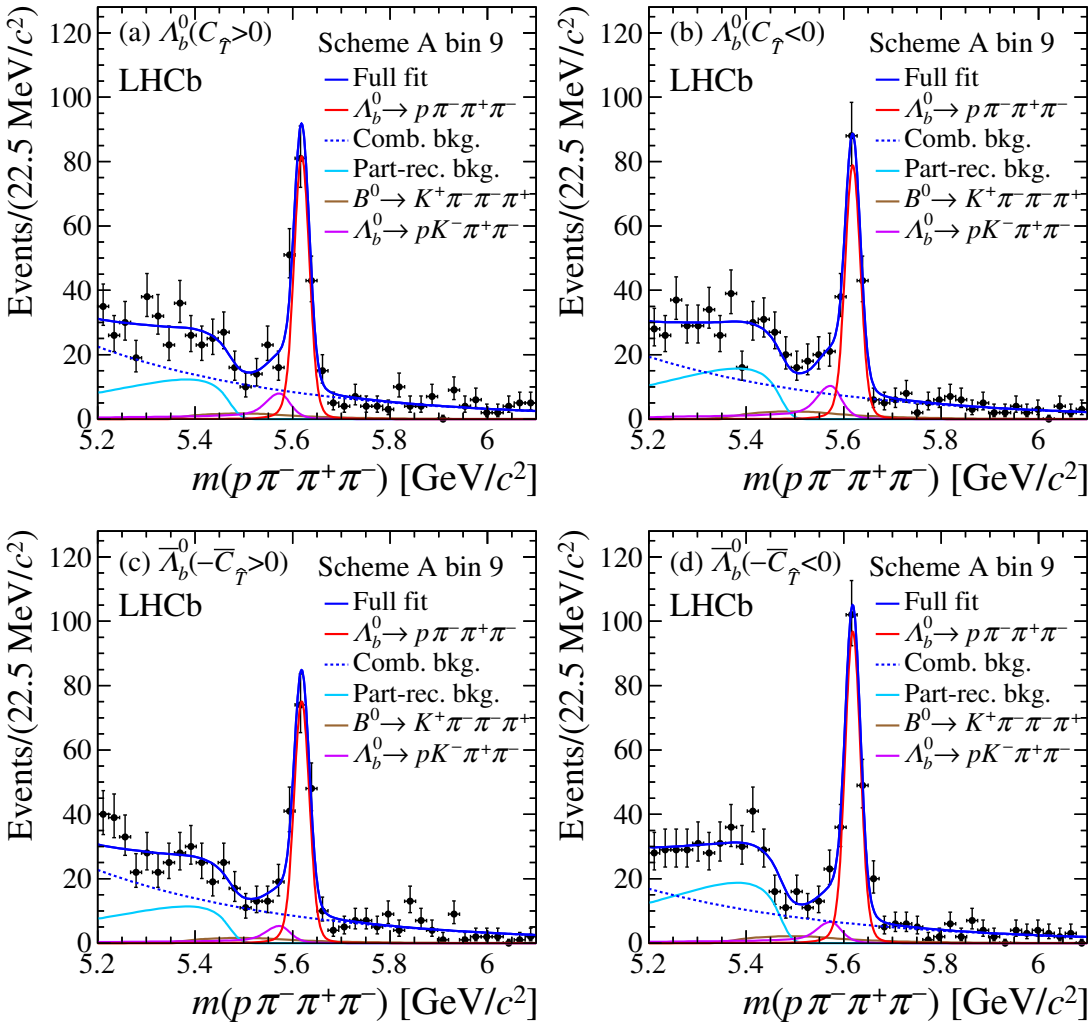

Figure 19: Projections of the unbinned maximum likelihood fit to the $\Lambda_b^0 \to p\pi^-\pi^+\pi^-$ decays in bin 9 in scheme A.

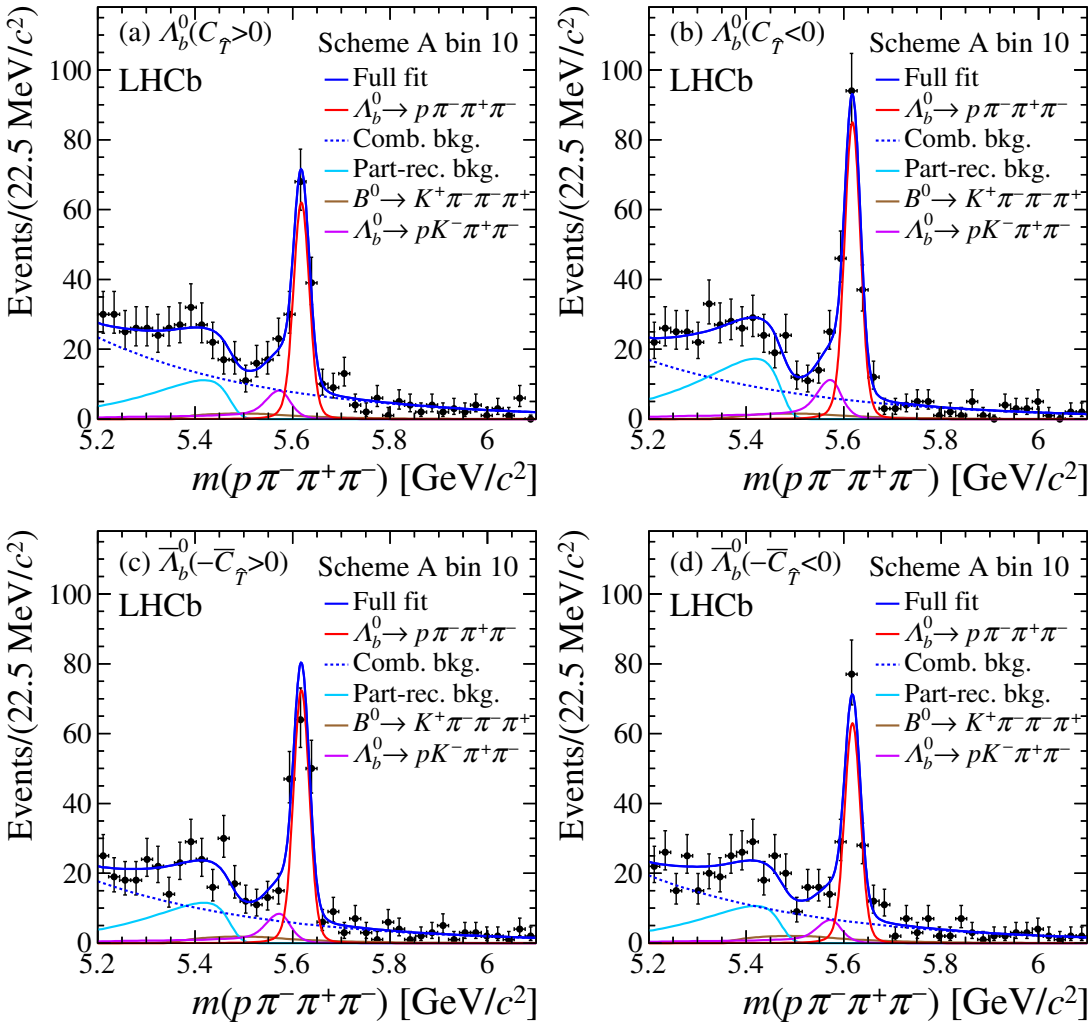

Figure 20: Projections of the unbinned maximum likelihood fit to the $\Lambda_b^0 \to p\pi^-\pi^+\pi^-$ decays in bin 10 in scheme A.

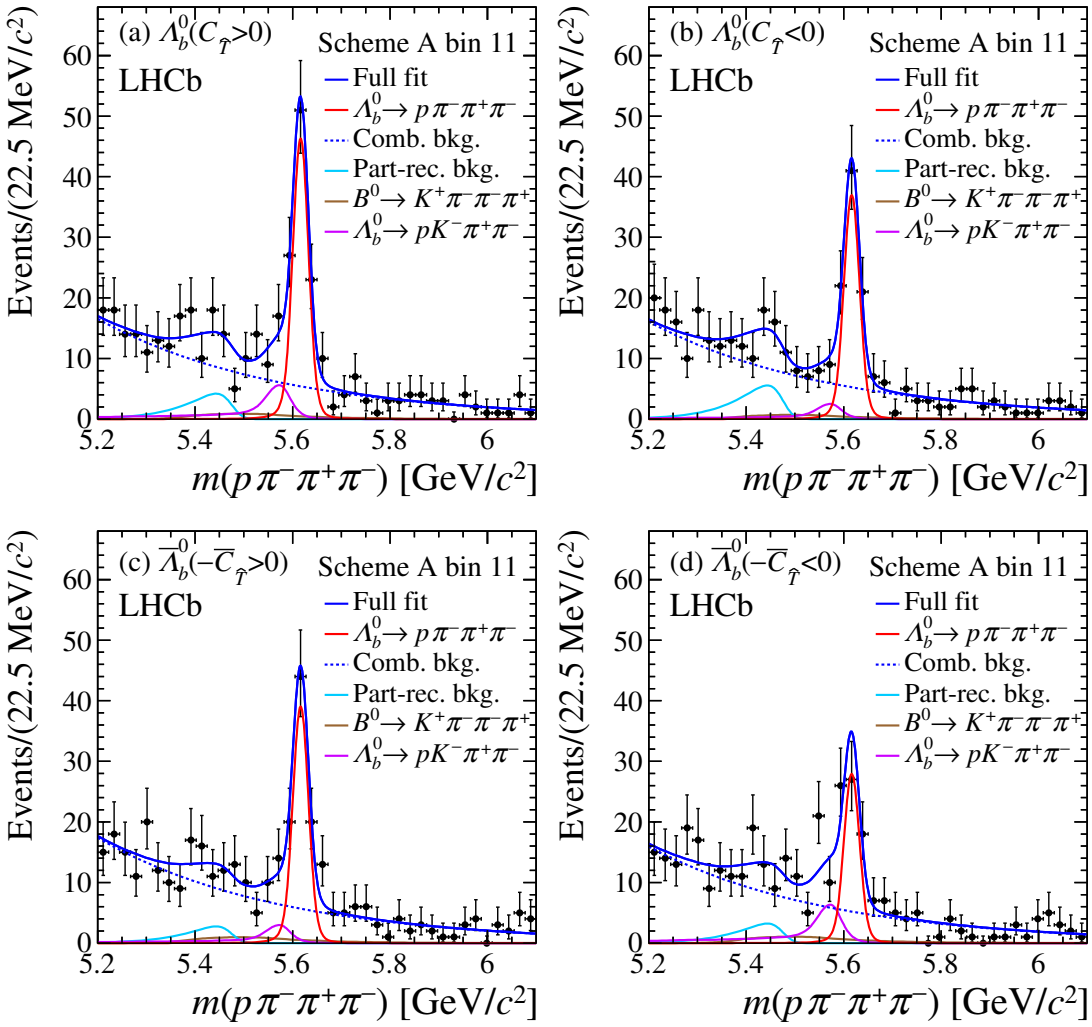

Figure 21: Projections of the unbinned maximum likelihood fit to the $\Lambda_b^0 \to p\pi^-\pi^+\pi^-$ decays in bin 11 in scheme A.

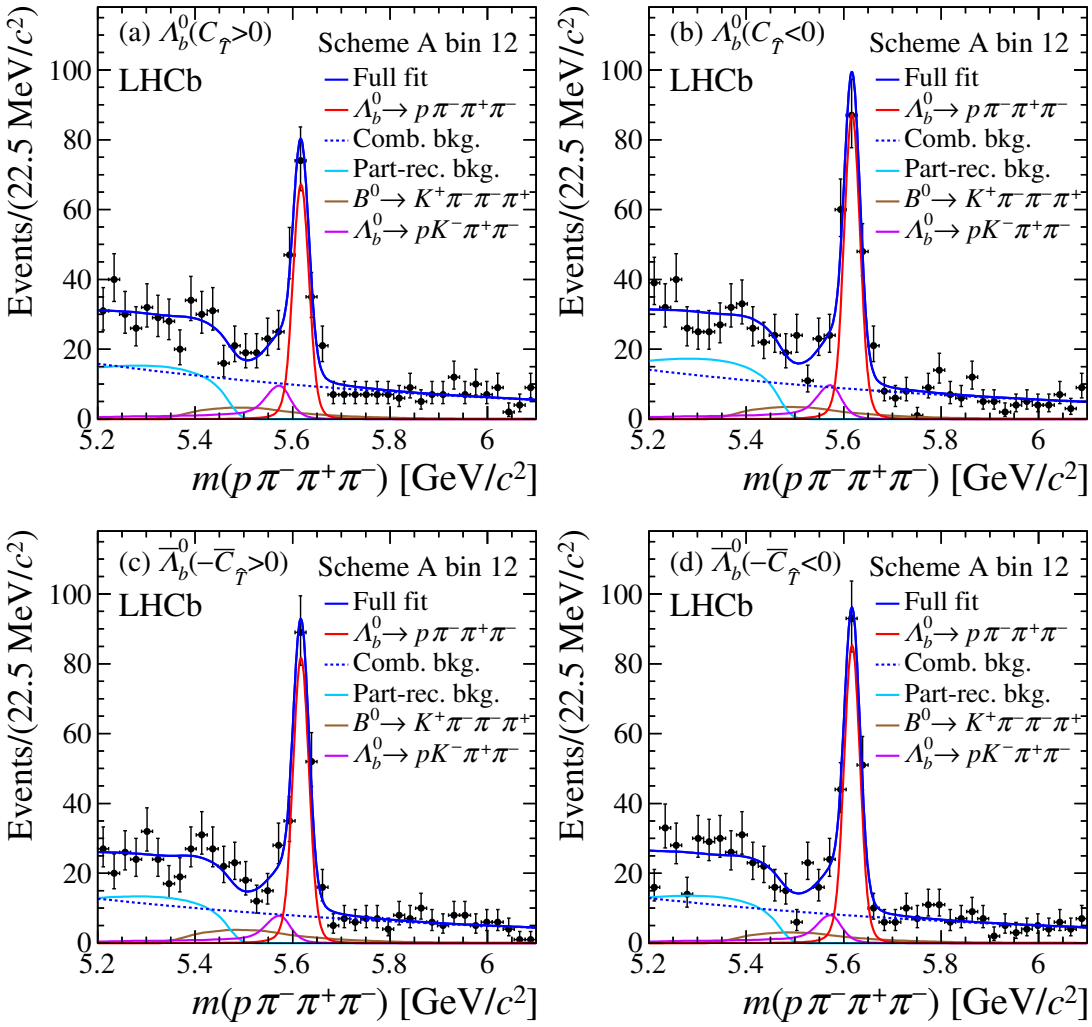

Figure 22: Projections of the unbinned maximum likelihood fit to the $\Lambda_b^0 \to p\pi^-\pi^+\pi^-$ decays in bin 12 in scheme A.

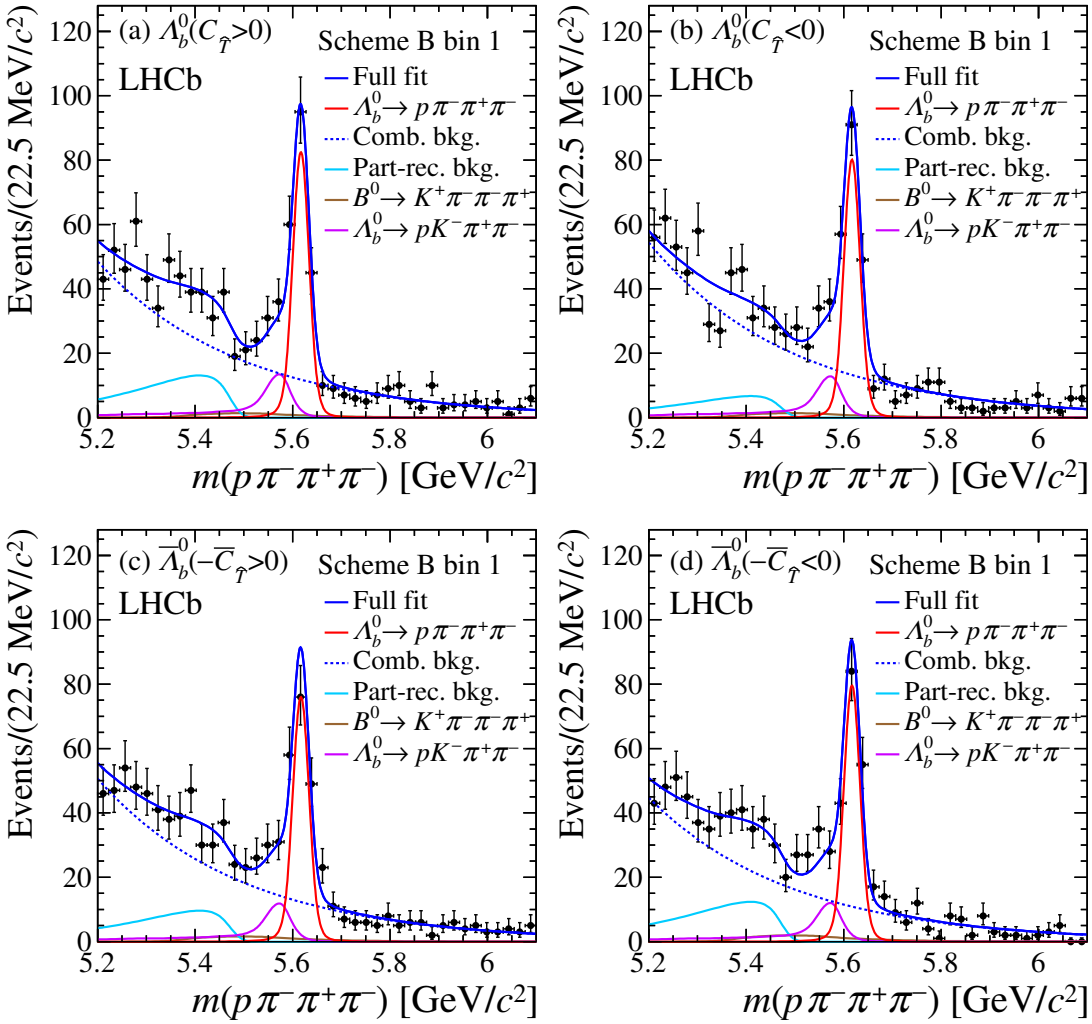

Figure 23: Projections of the unbinned maximum likelihood fit to the $\Lambda_b^0 \to p\pi^-\pi^+\pi^-$ decays in the region $0 < |\Phi| < \pi/10$, corresponding to bin 1 in scheme B.

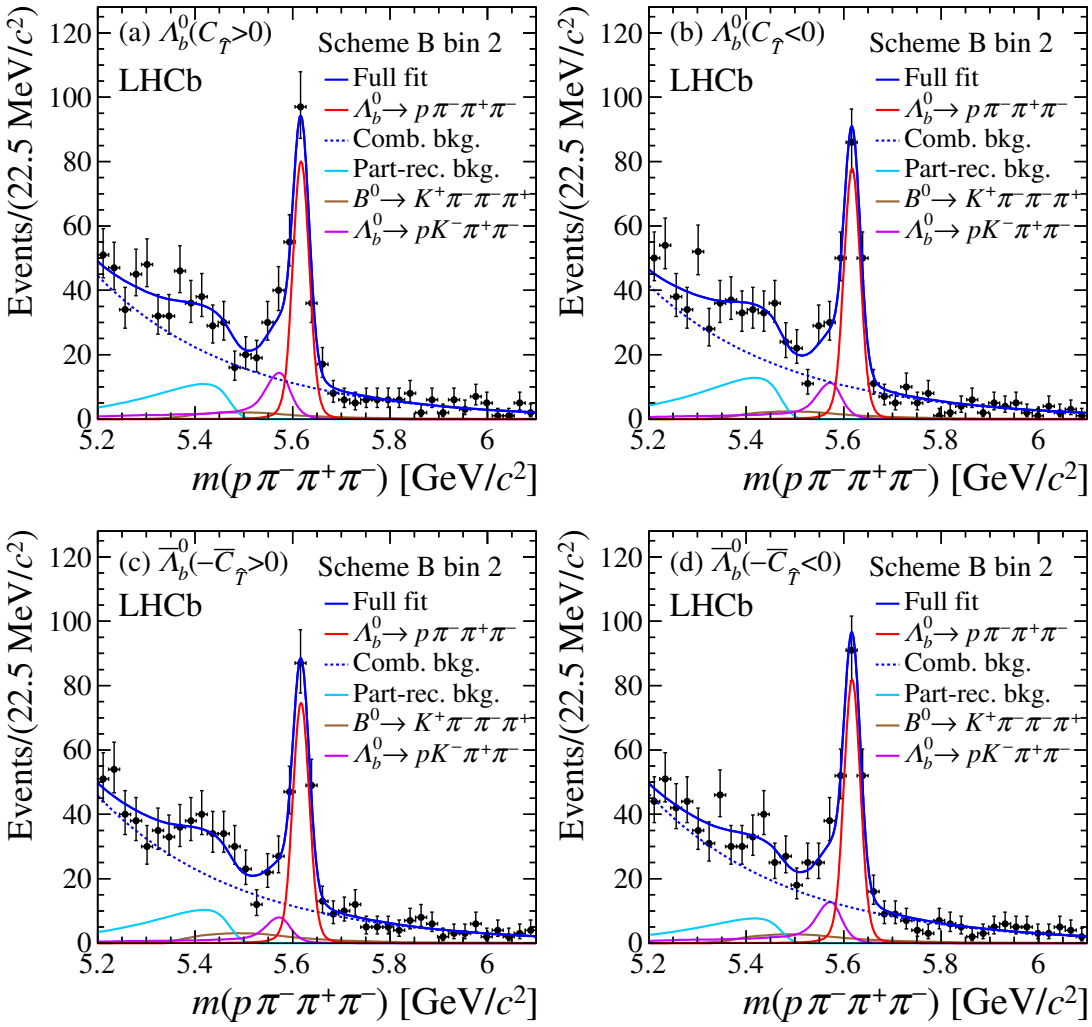

Figure 24: Projections of the unbinned maximum likelihood fit to the $\Lambda_b^0 \to p\pi^-\pi^+\pi^-$ decays in the region $\pi/10 < |\Phi| < 2\pi/10$, corresponding to bin 2 in scheme B.

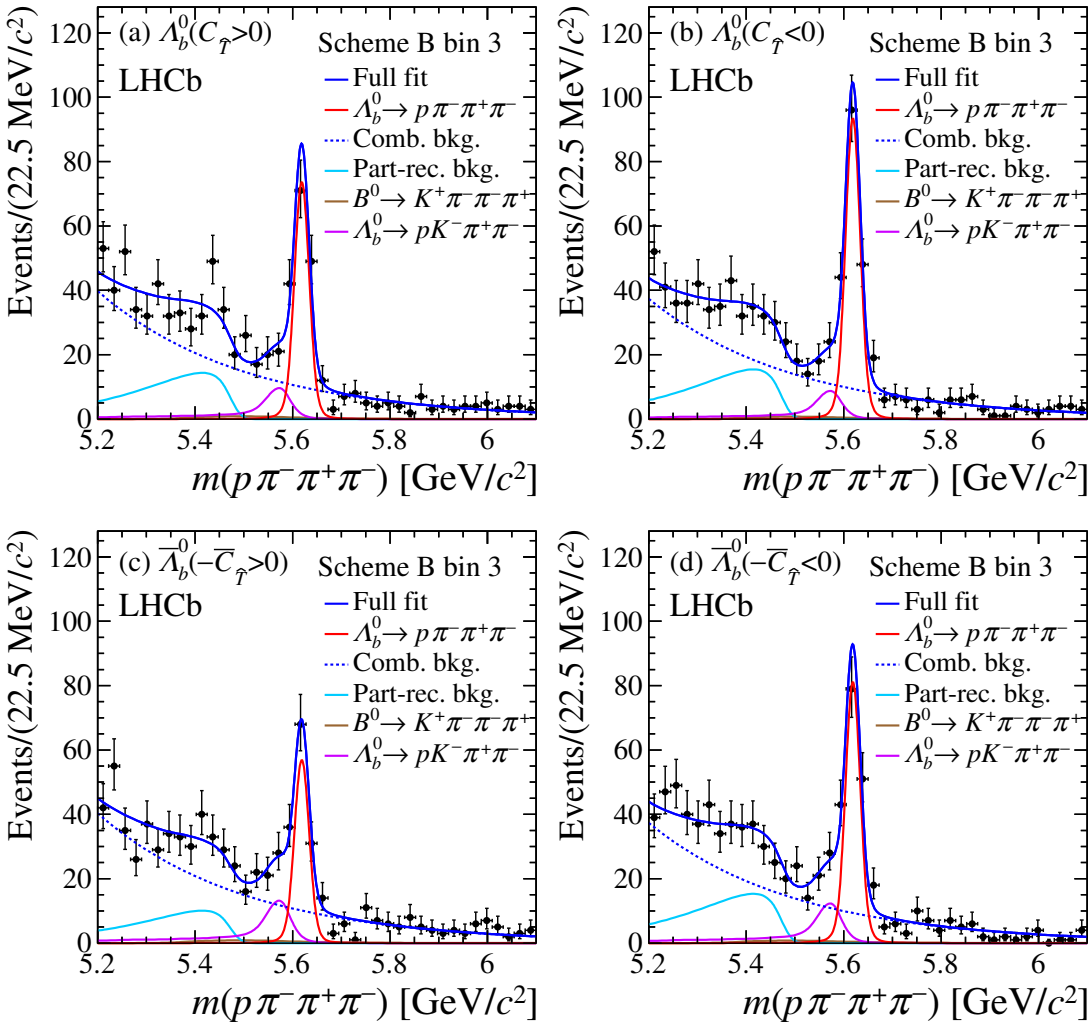

Figure 25: Projections of the unbinned maximum likelihood fit to the $\Lambda_b^0 \to p\pi^-\pi^+\pi^-$ decays in the region $2\pi/10 < |\Phi| < 3\pi/10$, corresponding to bin 3 in scheme B.

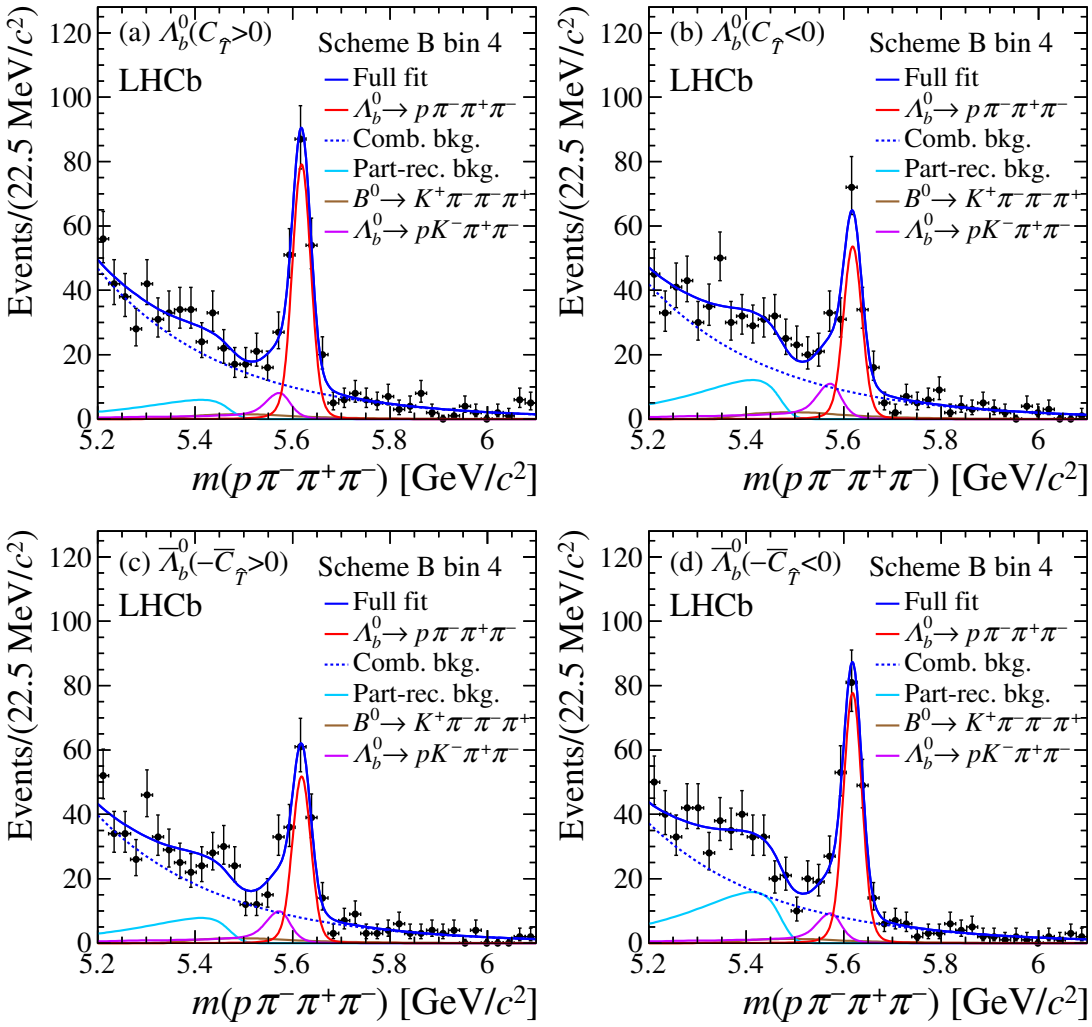

Figure 26: Projections of the unbinned maximum likelihood fit to the $\Lambda_b^0 \to p\pi^-\pi^+\pi^-$ decays in the region $3\pi/10 < |\Phi| < 4\pi/10$, corresponding to bin 4 in scheme B.

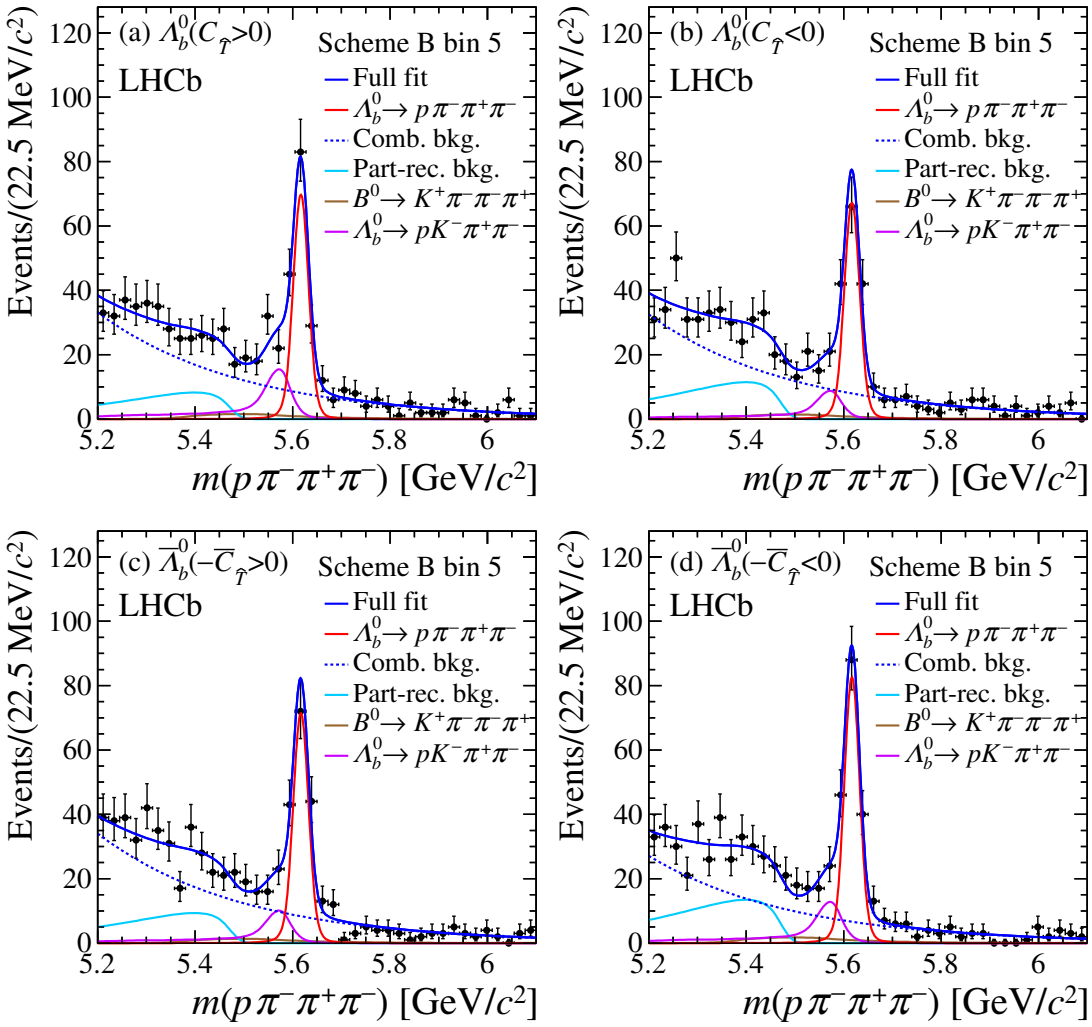

Figure 27: Projections of the unbinned maximum likelihood fit to the $\Lambda_b^0 \to p\pi^-\pi^+\pi^-$ decays in the region $4\pi/10 < |\Phi| < 5\pi/10$, corresponding to bin 5 in scheme B.

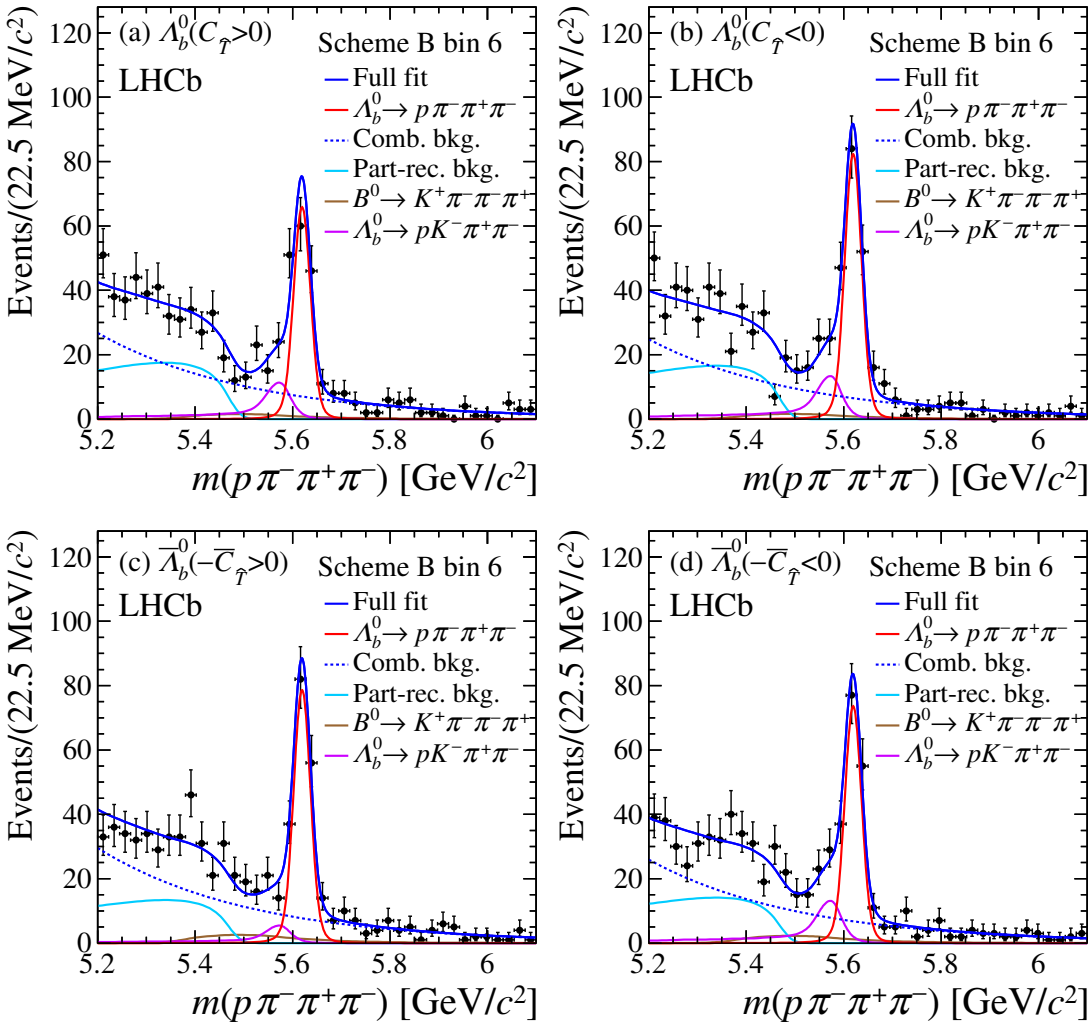

Figure 28: Projections of the unbinned maximum likelihood fit to the $\Lambda_b^0 \to p\pi^-\pi^+\pi^-$ decays in the region $5\pi/10 < |\Phi| < 6\pi/10$, corresponding to bin 6 in scheme B.

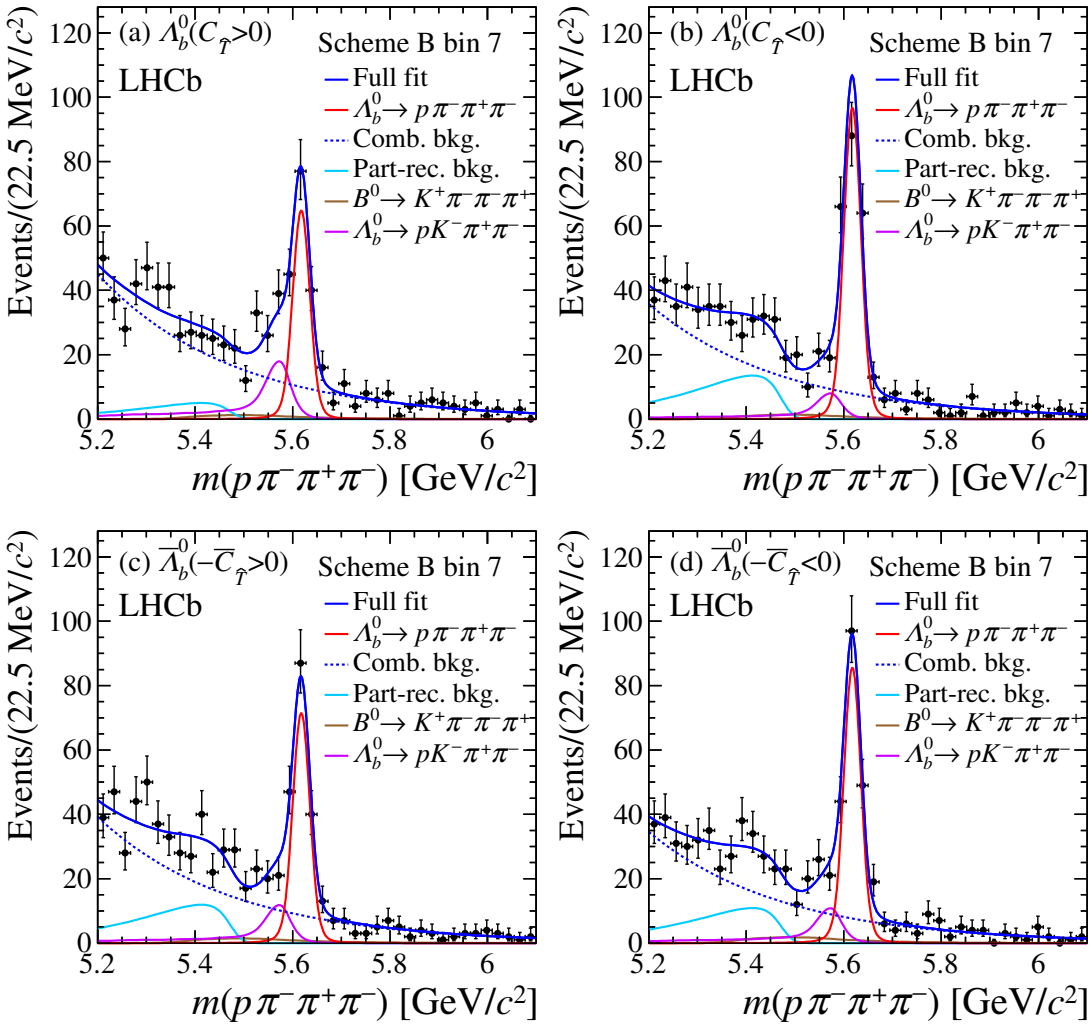

Figure 29: Projections of the unbinned maximum likelihood fit to the $\Lambda_b^0 \to p\pi^-\pi^+\pi^-$ decays in the region $6\pi/10 < |\Phi| < 7\pi/10$, corresponding to bin 7 in scheme B.

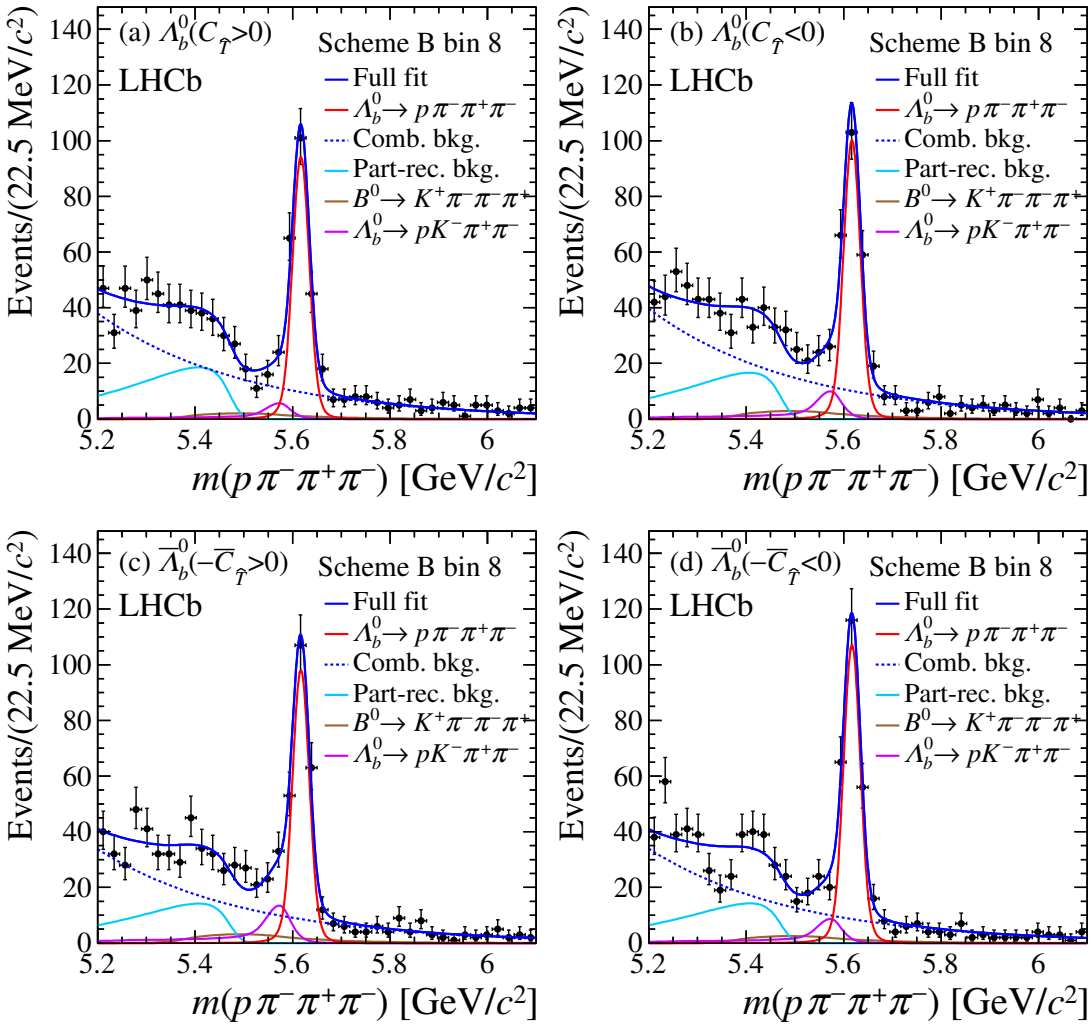

Figure 30: Projections of the unbinned maximum likelihood fit to the $\Lambda_b^0 \to p\pi^-\pi^+\pi^-$ decays in the region $7\pi/10 < |\Phi| < 8\pi/10$, corresponding to bin 8 in scheme B.

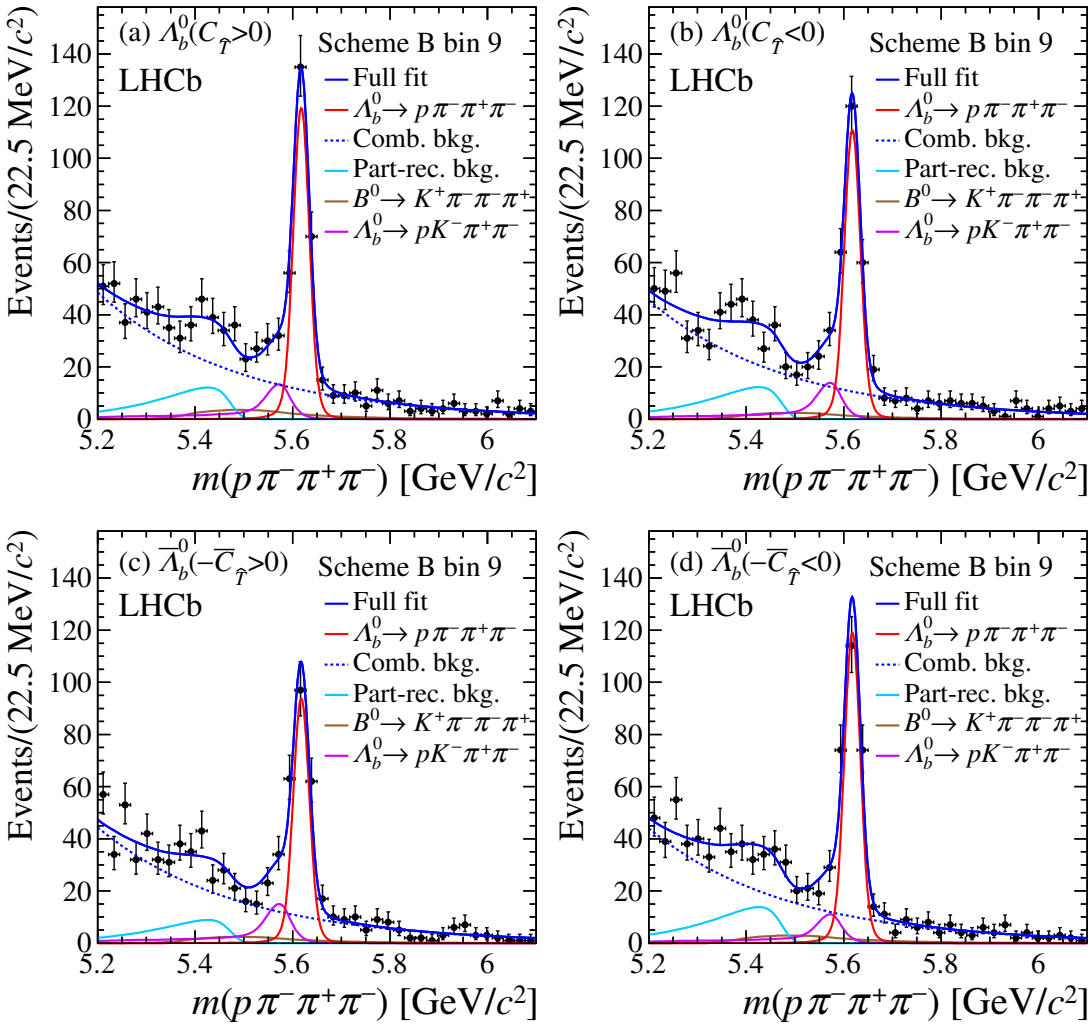

Figure 31: Projections of the unbinned maximum likelihood fit to the $\Lambda_b^0 \to p\pi^-\pi^+\pi^-$ decays in the region $8\pi/10 < |\Phi| < 9\pi/10$, corresponding to bin 9 in scheme B.

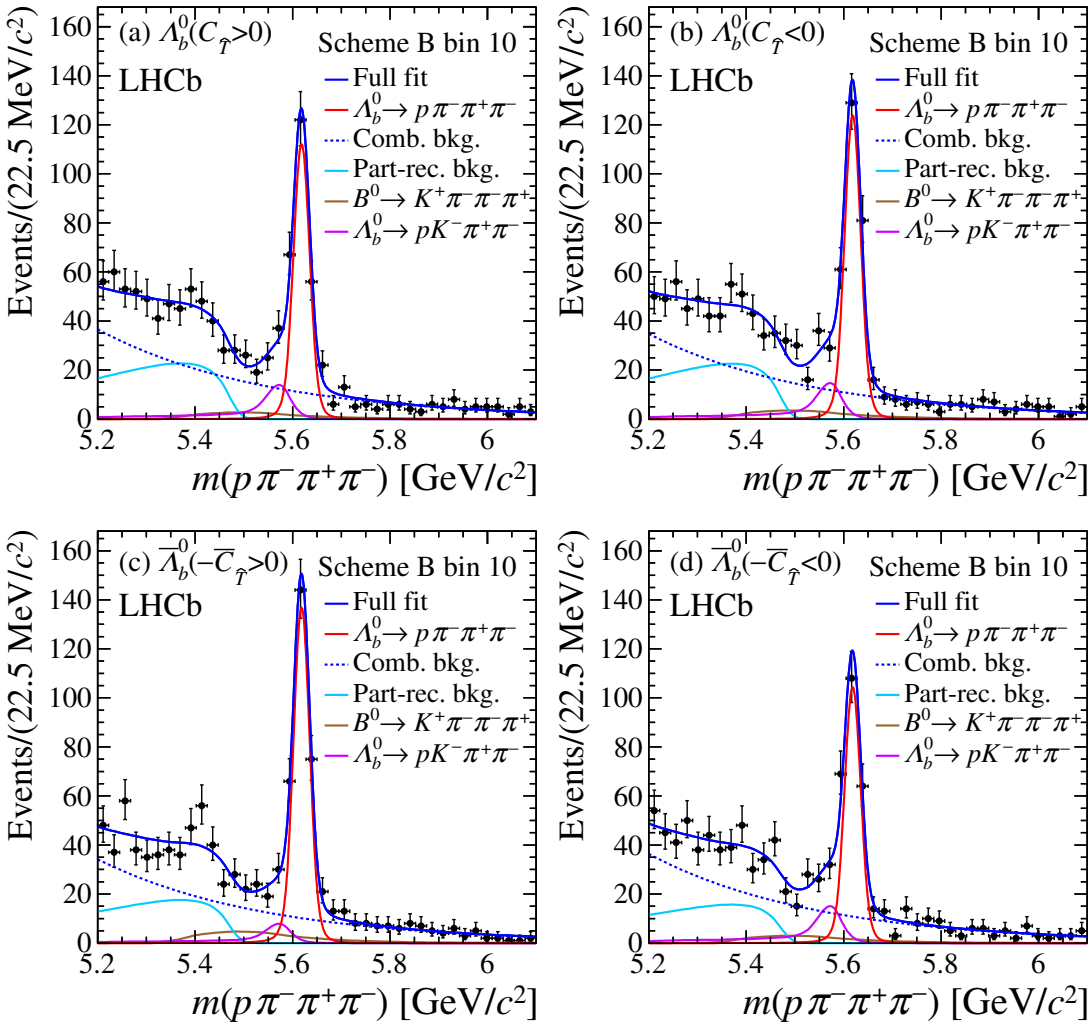

Figure 32: Projections of the unbinned maximum likelihood fit to the $\Lambda_b^0 \to p\pi^-\pi^+\pi^-$ decays in the region $9\pi/10 < |\Phi| < \pi$, corresponding to bin 10 in scheme B.

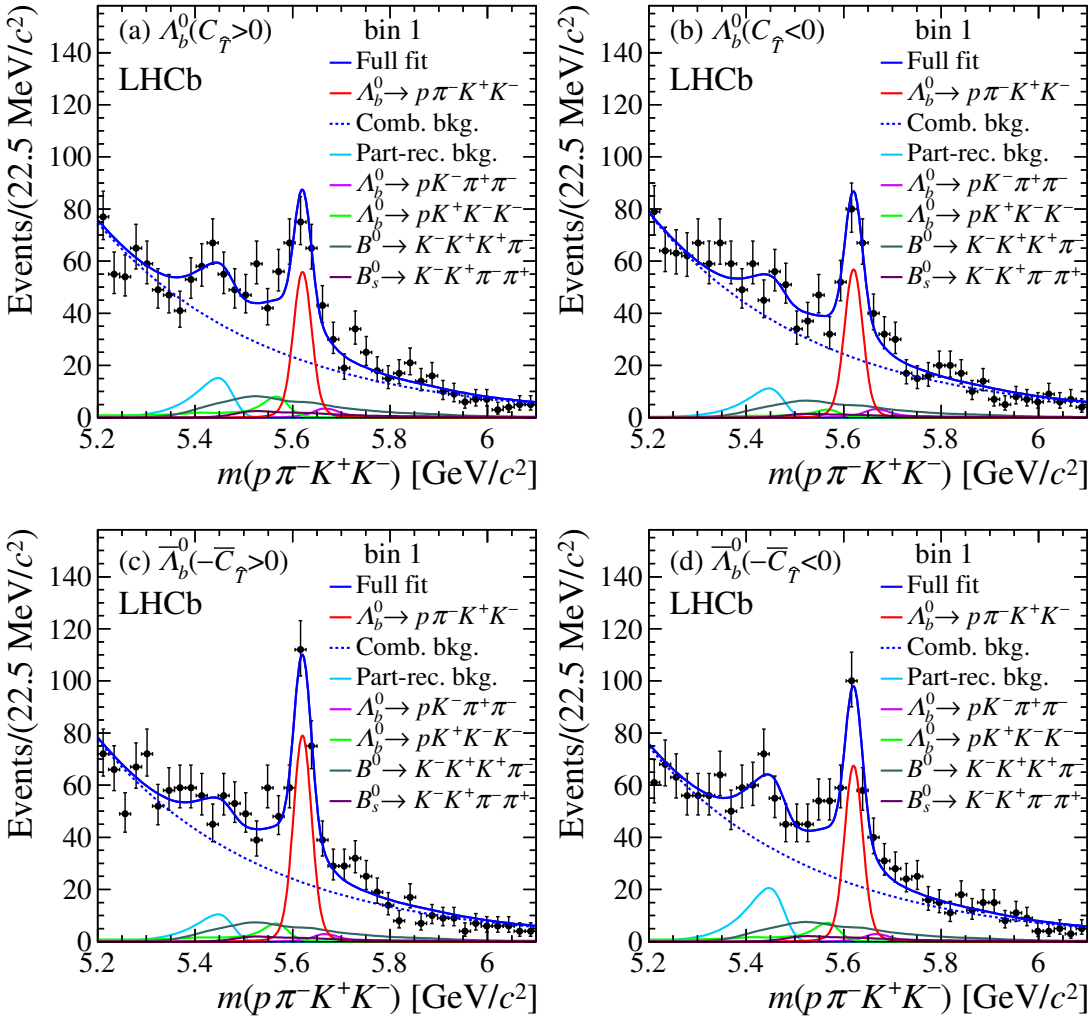

Figure 33: Projections of the unbinned maximum likelihood fit to the $\Lambda_b^0 \to p\pi^- K^+ K^-$ decays in bin 1.

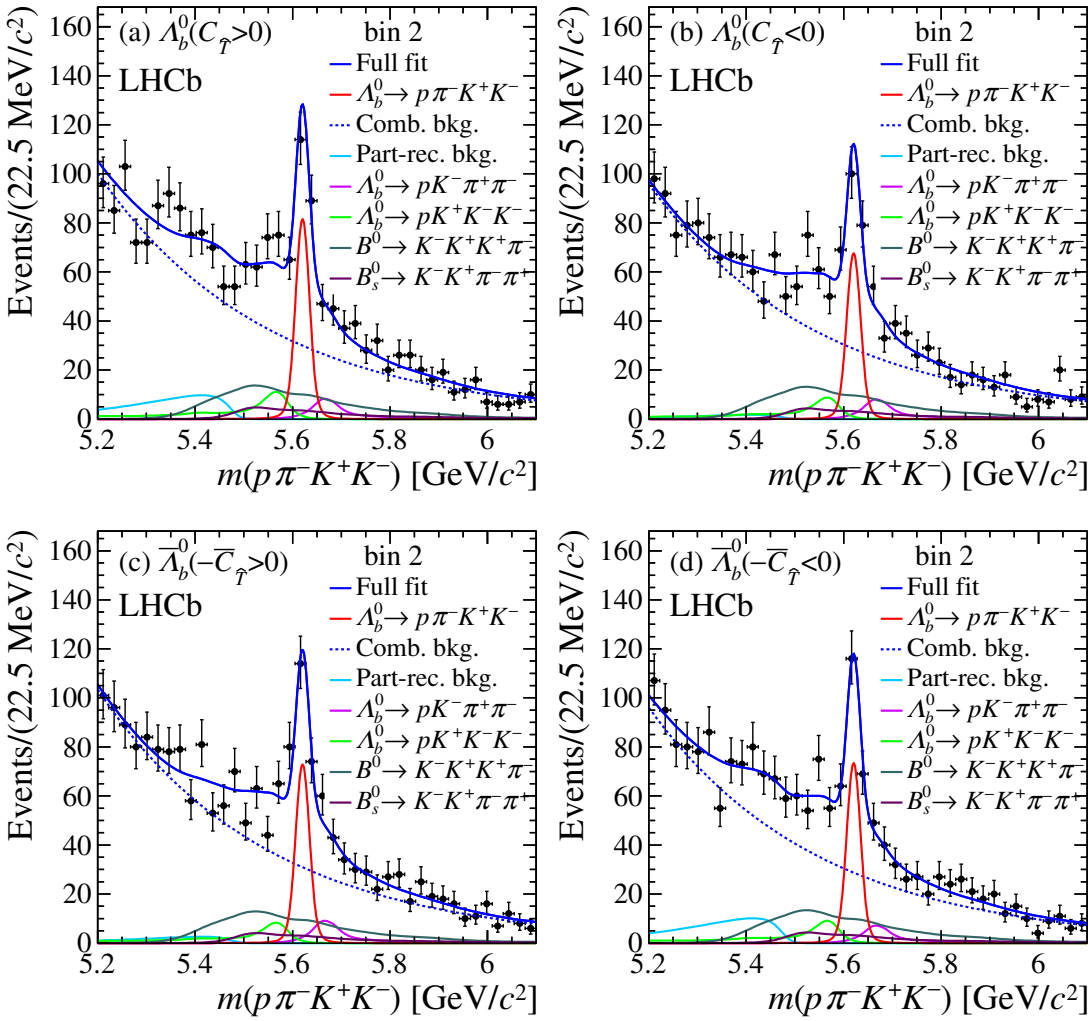

Figure 34: Projections of the unbinned maximum likelihood fit to the $\Lambda_b^0 \to p\pi^-K^+K^-$ decays in bin 2.

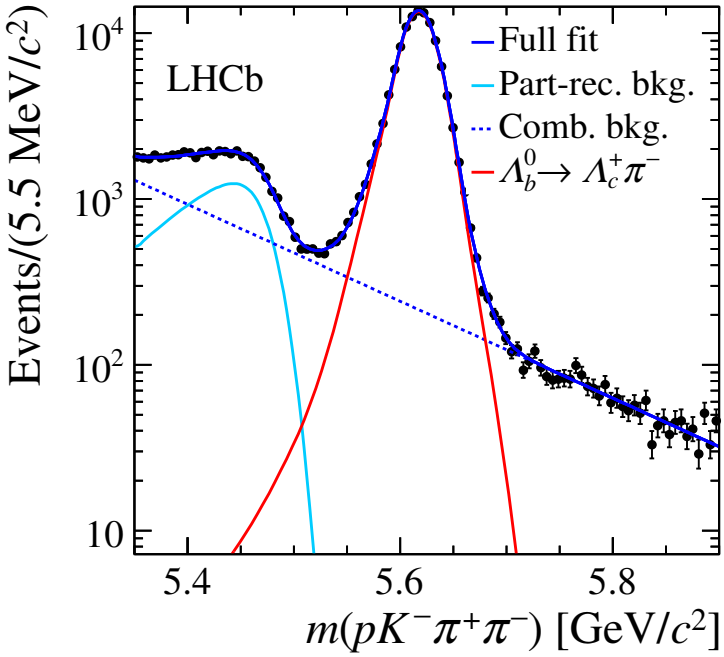

Figure 35: The invariant mass distribution of the $\Lambda_b^0 \to \Lambda_c^+(\to pK^-\pi^+)\pi^-$ candidates, which constitutes a control sample for this analysis. A binned maximum likelihood fit is overlaid on the data points as a blue curve. The contribution of each component is represented by a line as shown in the legend.

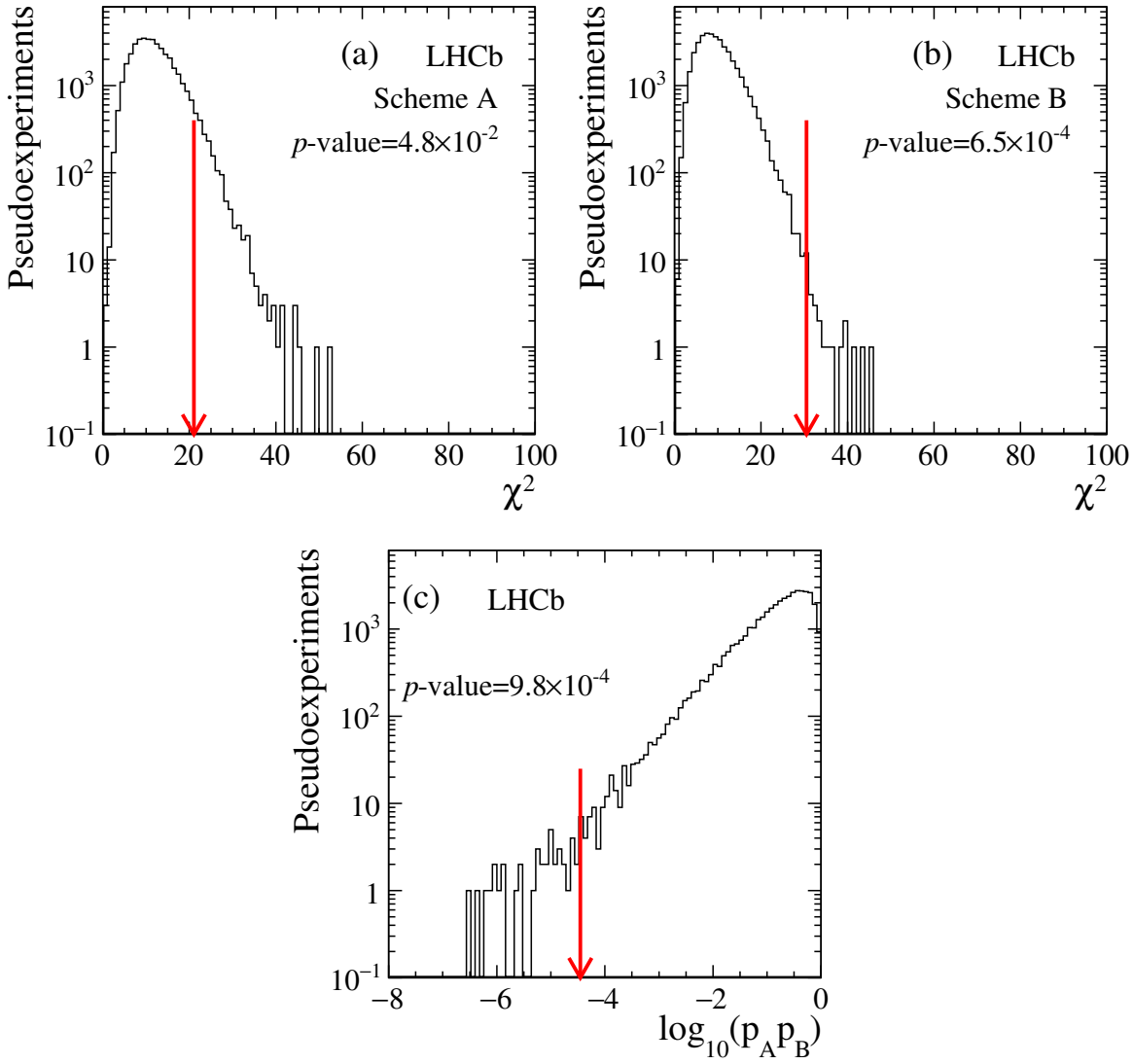

Figure 36: The χ^2 distributions obtained using 40,000 pseudoexperiments with *CP* symmetry for (a) scheme A, and (b) scheme B; and (c) the distribution of the $\log_{10}$ of the product of the p-values of schemes A and B.